ROBOTICS AND MECHATRONICS

Embedded thrust estimator design of a brushless direct current motor used in multi-rotor Unmanned aerial vehicle

R. (Roshal) Nikhil Menezes

MSC ASSIGNMENT

Committee:
R.A.M. Hashem, MSc
prof. dr. ir. G.J.M. Krijnen
dr. ir. W.B.J. Hakvoort

September, 2019

041RaM2019
Robotics and Mechatronics
EEMathCS
University of Twente
P.O. Box 217
7500 AE Enschede
The Netherlands

UNIVERSITY OF TWENTE. | TECHMED CENTRE

UNIVERSITY OF TWENTE. | DIGITAL SOCIETY INSTITUTE

Summary

The interaction of multi-rotor UAVs with the environment is an active topic of research. The interaction tasks include wall painting, crack detection, corrosion detection, and inspection tasks. The interaction tasks require precision force control. Many existing system's in the literature use an open-loop static map for thrust control design, a small change in thrust will result in inaccurate tasks. In this research, an embedded thrust estimator design is proposed based on the systems physical model along with using the rotors acceleration and motor current acquired from embedded sensors. The outcome of this research is to select an ESC which has inbuilt motor current and rotor angular velocity sensing. To study the influence of the wind disturbance on a BLDC rotor system used in multi-rotor UAV. The disturbance is created by blocking objects or in the presence of another rotor. This work is an important step towards having a closed-loop thrust controller designed to have precise thrust forces.

Contents

List of Acronyms

AOA	Angle of Attack
AOI	Angle of Incidence
BLDC	Brushless Direct Current Motor
CPU	Central Processing Unit
CRC	Cyclic redundancy check
DMA	Direct memory Access.
ESC	Electronic speed Controller
FC	Flight Controller
FTDI	Future Technology Devices International
GE	Ground effect
GPS	Global positioning system
GUI	Graphical User Interface
IMU	Inertial measuring Unit
IGE	In ground effect
LAN	Local Area Network
MCU	Micro Controller Unit
OGE	Out of ground effect
PPM	Pulse Position Modulation
PWM	Pulse Width Modulation
RAM	Robotics And Mechatronics
UAV	Unmanned Areal Vehicle

List of Notations

Below is the summary of the notations used in this thesis,

ρ the density of air
A the propeller area
ω the angular velocity of the propeller.
c_l the rotor lift coefficient.
σ the solidity ratio.
C_p Power coefficient.
C_d Drag coefficient.
C_r Propeller torque coefficient.
T Thrust.
T_i ideal thrust.
τ_d Propeller drag torque.
τ_{d_i} ideal propeller drag torque.
R radius of the propeller.
C chord length of the blade.
r_m the mean radius.
N number of propeller blades
T_{GE} thrust generated in proximity to the ground.
T_{FA} thrust generated in free air.
Z propeller height above ground.
B propeller scaling parameter, B =1 for helicopter.
D rotor diameter.
$\frac{k}{k_\infty}$ Induced power ratio IGE to OGE.
ρ Estimated parameter from experimental data obtained from hovering the quad-copter at different level.
$\hat{T}$ Estimated thrust.
$\hat{\tau}_d$ Estimated drag torque.
$\hat{\dot{\omega}}$ Estimated rotor angular acceleration.
$\hat{\omega}$ Estimated rotor angular velocity.
k_t Motor Torque Constant
I Motor inertia
V Motor voltage
i Motor current
T_d Motor desired thrust
ω Rotor angular velocity

1 Introduction

1.1 Context and problem statement

A multi-rotor UAV is a small-scale electrically powered aerial vehicle that use number of rotors for propulsion [1]. Multi-rotor UAVs are becoming increasingly popular in the area of photography, military, agriculture, express industry, survey, infrastructure management, forestry, and fisheries [2]. All these UAVs are designed for free flight.

In recent years among the active research, the interaction of UAVs with the environment is one of the most promising fields because of its potential applications. The interaction tasks include wall painting [3] [4], wall interaction[5], crack detection, weld inspection, corrosion detection[6][7], writing[1], wind turbine blade inspection[2] and window cleaning drones[3]. These tasks lead to investigate various designs which are suitable for physical interaction [4].

Problem 1: Conventional UAVs, have their rotors pointing, upwards resulting in under-actuated design. i.e, they cannot translate horizontally without rolling or pitching; this limits physical interaction tasks. One of the solutions would be using a tilted rotor model shown in Figure 1.1. Though the solution overcomes the under-actuation problem, it has one drawback. Such design creates aerodynamic interference's between the rotors that face each other, causing additional air-flow through these propellers which results in a thrust change.

(a) BetaX, a fully actuated hexacopter with an end-effector attached

(b) Holocoptor prototype of a quadcopter with a tilted rotor design [8].

Figure 1.1: Fully actuated multi-rotor UAVs with tilted rotor.

Problem 2: During interaction tasks, the UAVs are near the environment in which they interact, resulting in blocking the air-flow of the rotors that are facing the blocked object. The air-flow velocity through the rotor varies, changing the thrust. Figure 1.2a shows the UAV in a close environment with a wall. The UAVs, working in confined space for inspection tasks has a outcome similar to interaction tasks because of the regeneration of air-flow generated by the propellers. Figure 1.2b shows the UAV in limited space.

[1] https://www.youtube.com/watch?v=d81AzW_dHNg&t=1s
[2] https://www.youtube.com/watch?v=5JlirWpqgTw
[3] https://www.aerones.com/eng/cleaning_drone/

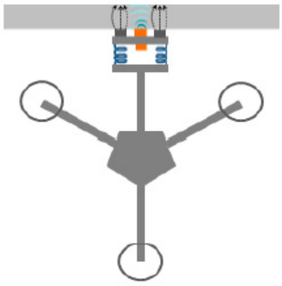

(a) Schematic of wall-sticking UAV for Non-Destructive ultrasonic and corrosion testing [6].

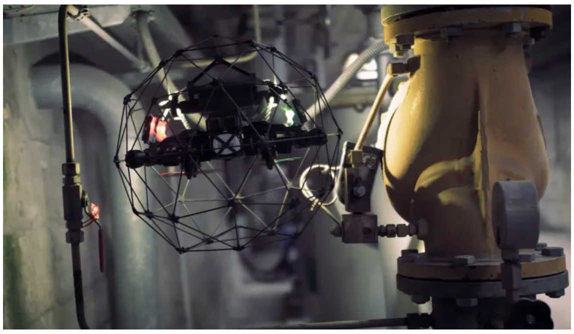

(b) Elios 2 UAV inspecting corrosion in the valve in confined space [7].

Figure 1.2: Multi-rotor UAVs working close to the wall.

Problem 3: UAVs during the inspection of a wind turbine blade, cleaning windows or flying outdoor are affected by a sudden gust; this varies air-flow velocity into the propeller blades which results a varying thrust produced by the rotors.

The problem could be summarized as: *"The existing UAV model uses a static map that converts the desired thrust to a motor PWM signal in an open-loop manner. A static map is measurement of thrust, when PWM duty cycle is between 0 to 100 percent in the absence of disturbances. For any aerodynamic change that occurs due to problems 1, 2, and 3, thrust remains unchanged because of the static map. Conventional UAVs, used for flying, work fine with a static map. However, while performing interaction tasks, the UAV needs to hover, which requires precision measurement of thrust."*

The proposed solution in this work would be creating a closed-loop thrust control system that rejects the disturbances. One solution would be a direct measurement of thrust using the force sensor, this is not a good solution because in dynamic situation where UAV performs interaction tasks the force sensors will also measure the contact forces and moments. The second solution is to estimate the thrust based on the physical model of the rotor. In the next section, the related work done in solving the issue is discussed.

1.2 Related Work

The author in [9] proposed a thrust sensing method for small UAVs using a strain gauge. The model suffered from a high signal to noise ratio at a sample rate of 200hz. The author in [10] [11] designed a force sensor, mounted between the BLDC motor and UAV frame to directly measure the forces, and pitch-roll torques. Using an external sensor to measure thrust adds additional sensors to UAV depending on the amount of rotors used; each rotor requires one sensor. Leading to additional power consumption and an increase in the weight of the UAV.

The authors in [1] [12] [13] designed a static model that relates thrust to the rotor angular velocity [4]. The model is effective for a wide range of applications in conventional UAVs but shows significant error while performing interaction tasks and in the presence of gust.

The authors in [14] proposed a wind speed estimation method to compensate wind disturbances due to gust using a single pitot tube to measure the forward velocity of UAV. The measurements obtained under 2m/s where unreliable; also, wind estimation of multi-rotor is challenging because of wind direction. The authors in [15] used four pitot tubes mounted underneath each rotor of the quadcopter to measure the axial velocity of the measurement. The estimated velocity measurement showed an error of 20 percent.

[4] This relation is discussed in chapter 2 equation 2.1

1.3 Proposed method

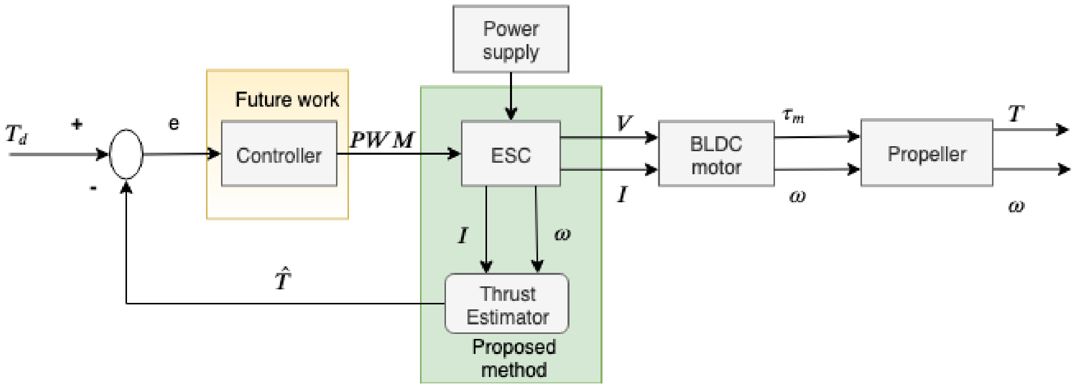

Figure 1.3: Proposed model showing thrust estimator design

In this thesis, I propose a model-based approach to estimate the thrust generated by a rotor using an embedded ESC that measures current and rotor angular velocity. Figure 1.3 shows an overview of the proposed method[5]. For accurate results, a BLDC motor, ESC, and the propeller are used for the experiments. The proposed method is divided into three goals,

1. *"Selection of a ESC, based on working protocol and embedded sensing."*
2. *"Analyze the effect of disturbances on a BLDC rotor system."*
3. *"Design of a thrust estimator using a model-based approach. Two design approaches are used in this research."*

The advantages of using a embedded thrust estimator are,

1. An ESC having embedded system will not change the aerodynamics of actual multi-rotor system.
2. It is free from mechanical noise.
3. Faster communication between the FC and ESC and lesser communication error [6].

1.4 Report outline

The report is divided into six chapters, chapter one, is an introduction which explains the problem, related work, and proposed solution. In the second chapter, the background related to this research is explained. In chapter three, a survey is done on already existing ESCs, to select a suitable ESC. In chapter four, experiments are carried to know the influence of disturbances due to blocking object or air-flow creating objects on an BLDC rotor. In chapter five, two thrust estimator are designed. Finally, the conclusion and future work are discussed in chapter six.

[5]This method will be discussed in chapter 5
[6]Discussed in chapter 3

2 Background

The background knowledge required for the thesis is discussed in this section. It as three sections namely, Aerodynamics fundamental's, a study of disturbance's that affect thrust, and basic principle behind the BLDC motor is described in detail.

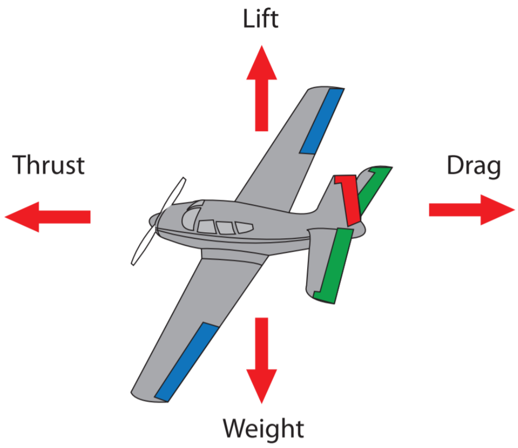

Figure 2.1: Four forces of flight [16]

2.1 Forces acting on a flying object

The four aerodynamic forces acting on any flying object are thrust, drag, lift and weight. In our case we consider the flying object as the multi-rotor UAV, it can be an quadcopter, an hexacopter or an octacopter. The UAV used in the RAM lab is a fully actuated hexacopter UAV. The forces and their direction of motion is shown in Figure 2.1.

- Lift: It is the vertical upward force, which overcomes or opposes the downward force occurred due to weight, is produced by the air which is flowing through the airfoil, and acts perpendicular to the flight path [17][18].
- Weight: It is the total load of a UAV. It pulls the UAV downward due to gravitational force.
- Thrust: The thrust is a forward force produced by the propeller or rotor [19]. It overcomes the drag force. However, for a hexacopter it is not always the case, this will be discussed in the section 2.1.3
- Drag: It is the opposing force caused by disruption of airflow by the propeller.

2.1.1 Lift

The lift is generated when the fluid changes its direction because of the obstruction created by an object or when the fluid is forced to move by the object passing through it [20]. In case of the hexacopter the object is the propeller and the fluid is air. The object can be moving in a stationary fluid or the fluid can flow through the stationary object. The lift can be generated by an airfoil depending on the factors like, density of the air, speed of the airflow, total area of the segment or airfoil and AOA between the air and the airfoil. To achieve an vertical upward lift the AOA of the airflow must be positive. At zero AOA, there is no lift in some airfoil like camber at zero AOA there is a positive lift [21] and at negative AOA, and negative lift is generated. Airfoil is a cross-sectional shape of a wing, propeller or blade [22].

The Figure 2.2 shows the basic concept behind the lift. When air hits the airfoil in positive AOA, the air gets split over and under the airfoil. This sudden change in the direction of the airflow causes an high and low pressure on the lower and upper surface of the airfoil. Due to this pressure gradient, and the viscosity of the fluid, the air in the upper surface will have high velocity then the lower surface. The production of lift is based on the Bernoulli's principle.

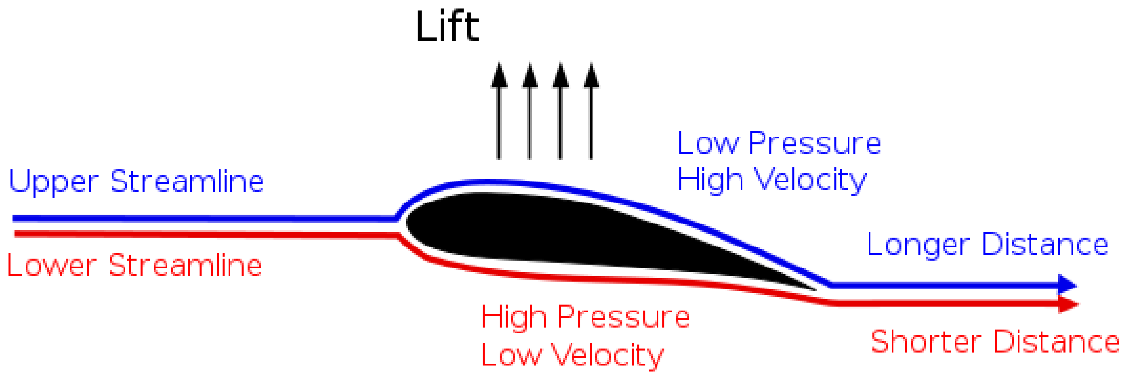

Figure 2.2: Lift produced by a airfoil [18]

- Bernoulli's Principle: This theory describes the relationship between the internal fluid pressure and fluid velocity [23]. It is based on law of conservation of energy and explains the lift force generated due to airfoil. An example is water running though a shower hose. In Figure 2.3, the flow of water through a tube is constant, neither accelerating or decelerating; hence the mass flow rate will be same at station 1, 2 and 3. The cross-sectional area of the station 2 is reduced, this will increase the water velocity to maintain a constant mass flow rate to maintain same amount of water flow through the reduced area. The velocity of the water flow will increase and pressure will decrease through the reduced area. This phenomenon is because of Venturi effect. The mass flow rate is the mass of flow per cross-sectional area of the tube.

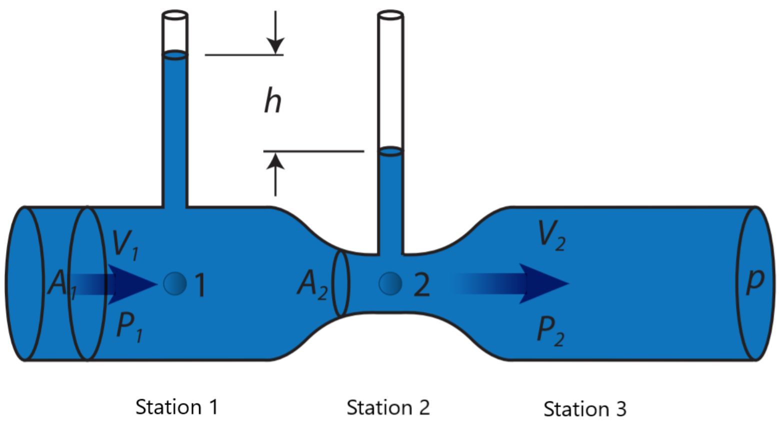

Figure 2.3: Flow of water through tube [24]

2.1.2 Weight

The weight is the total mass of the hexacopter and the gravitational pull from the earth surface. To lift the hexacopter the rotor's must generate enough lift. In this case, the object is the hexacopter whether it is at hovering position or on the ground position unless an external force is applied to lift. This can be achieved by increasing the speed of the motor more details is in section 2.1.5.

2.1.3 Thrust

When a system expels or accelerates mass in one direction, the accelerated mass will cause a force of equal magnitude but opposite direction on that system [25]. The thrust is the force that propels a flying object in the direction of motion. Like lift, thrust, is generated by the rotation of the main rotor system. In a hexacopter, thrust can be a forward, reward, side-ward, or vertical. The resultant of thrust and lift determines the direction of movement of the hexacopter [25].

2.1.4 Drag

The drag resists the movement of the hexacopter through air and is produced when a lift occurs. It is caused by friction and differences in air pressure. It flows parallel to the wind. To fly a hexacopter the drag must be overcome by the varying the speed of the rotor.

2.1.5 Ideal thrust, rotor torque and Aerodynamic power

UAV propulsion and lift is provided by the propeller's, which convert's rotation of the motors into thrust by accelerating a column of air. Using the Blade Element Method (BEM) the thrust, torque and power of a ideal rotor motion can be modelled [26]. The ideal condition is when the disturbances creating additional air flow through the rotor is neglected. The airflow can be due to the environment wind(gust), ground effect, wall effect, additional air flow caused due to tilting of propeller's. These instabilities caused during the flight is discussed in section 2.2. The ideal condition can also be called as a static method. For an ideal rotor of uniform airfoil profile thrust is given by [19] [26]:

$$T = C_t \omega^2 \tag{2.1}$$

where C_t is given by,

$$C_t = \frac{C_l \sigma \rho A R^2}{6} \tag{2.2}$$

The ideal propeller drag torque is given by,

$$\tau_r = C_r \omega^2 \tag{2.3}$$

where coefficient of propeller drag torque is given by,

$$C_r = (C_T \frac{\sqrt{C_T}}{2} + \frac{C_d \sigma}{8})(\rho A R^3) \tag{2.4}$$

Correspondingly, ideal rotor power is given by,

$$P = C_p \rho A \omega^3 R^3 \tag{2.5}$$

where C_p is given by,

$$C_p = C_r \Rightarrow P = \tau_r \omega \tag{2.6}$$

The ideal thrust generated by a BLDC motor can be increased by increasing the radius, angular velocity or solidity ratio of the rotor clearly visible from 2.1. The rotor solidity ratio is given by [27],

$$\sigma = \frac{c}{s} \Rightarrow \sigma = \frac{c}{2\pi \frac{r_m}{N}} \tag{2.7}$$

where mean radius is the average of the inner and outer radius of the blade. Rotor solidity ratio can be increased by adding additional blades to the rotor. However, there will be trade offs as changing these parameters also impacts rotor torque and power [28].

2.2 Study on different types of disturbance's

In this section, the disturbances affecting the thrust are investigated.

2.2.1 Ground effect

The ground effect is the change in thrust generated by a multi-rotor UAV when flying in close proximity to the ground. It is also called as cushion effect [29]. It is caused when the downward movement of air is blocked by the ground, more air molecules stay below the rotor wing and these increases the pressure below the rotor [30]. This will effect in achieving more thrust for a multi-rotor UAV. This aerodynamic phenomenon will lead to instability and unpredictable flight conditions [31]. The wake conditions for a rotor operating far away from the ground and close to the ground are shown in Figure 2.4. A wake is a downward air stream caused by the UAV due to density difference of air below and above the propeller.

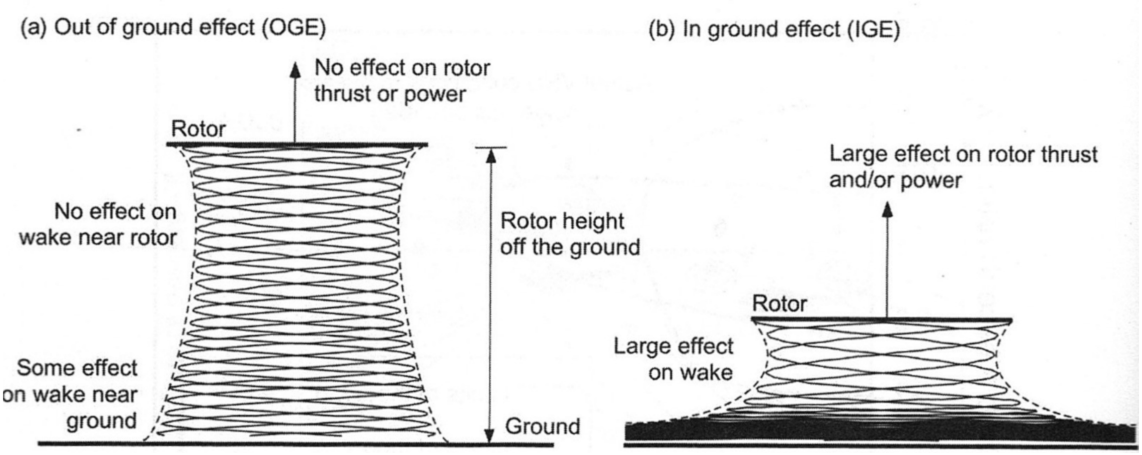

Figure 2.4: Rotor wake visualization far away from the ground and close to ground [19]

An analytic model of ground effect for a single rotor was developed by Cheesman and Bennett [32] for a helicopter. They used the experimental method, this involves a rotor near the ground with different distance from the ground. The relationship is given by:

$$T_{GE} = \frac{1}{1-(\frac{BR}{4z})^2} T_{FA} \tag{2.8}$$

2.2.2 Wall Effect

Similar to ground effect, the wall effect is due to close proximity with the wall. It is a well known in the research community but as yet under referenced in the literature. During the interaction of VTOL aircraft Heyson [33] experienced the wall effect. He showed that a additional thrust is generated by propellers while interfering with wall. J.P. (Just) van Westerveld [5] in his research on wall effect showed that there is a slight increase in thrust with increase in distance. Hence, there is a contradictory between Heyson and J.P. (Just) van Westerveld research which needs to be studied.

2.2.3 Tilting rotor Effect

The hexacopter model designed in RAM is a fully actuated UAV [34]. A fully actuated UAV is which all the dimension's are used in motion of flight. A tilted rotor method is implemented to design the fully actuated hexacopter UAV model. Due to tilting of the rotor's, two rotor's face each other this will effect in increase of air flow.

2.2.4 Tip Vortices

During lift, a part of the airflow exits the propeller and recirculate upwards, as shown in Figure 2.5. The circulation of the air in propeller blade tip is called as tip vortices [35]. The recirculating of air reduces the rotor ability to accelerate in air, producing less thrust. To achieve more efficiency ducted propeller's are used. In ducted propeller, a non-rotating nozzle is fitted across the propeller.

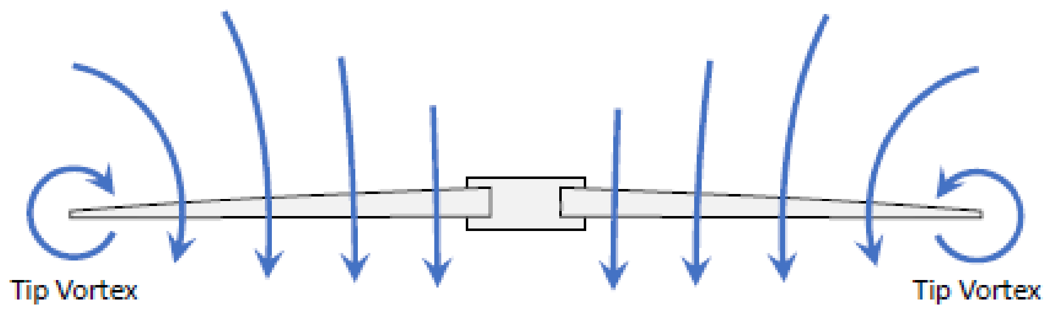

Figure 2.5: Tip vortices [36]

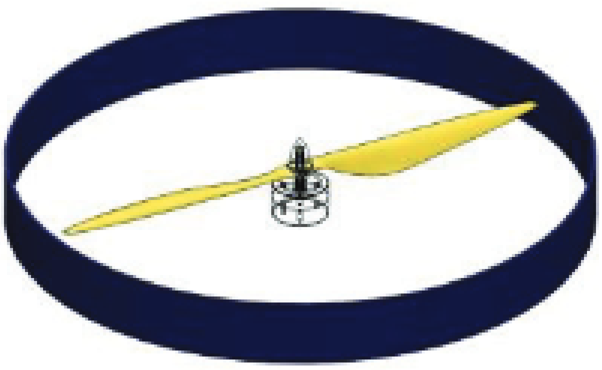

Figure 2.6: Ducted propeller [37]

2.3 BLDC motor

BLDC motors are referred to by many aliases: brush-less permanent magnet, permanent magnet ac motors, permanent magnet synchronous motors etc. As the name suggests BLDC motor does not use any brushes, the commutation of these motors take electronically. In this section we will study the working principle of a BLDC motor and its comparison with dc motor.

2.3.1 Working Principle

The BLDC motor as two main parts namely, a fixed or stationary part which is known as a stator and a moving part called rotor. The stator of BLDC motor coil winding's. Each of this winding's are spread over the stator peripherally to structure a pair of poles [38]. The rotor of BLDC motor is made up of a permanent magnet's mounted on a non-magnetic core or shaft. The number of poles on the rotor varies depending on the requirements. Higher the number of poles better torque while it reduces the maximum speed of the motor [39].

The working principle is based on interaction between two magnetic fields. By applying the

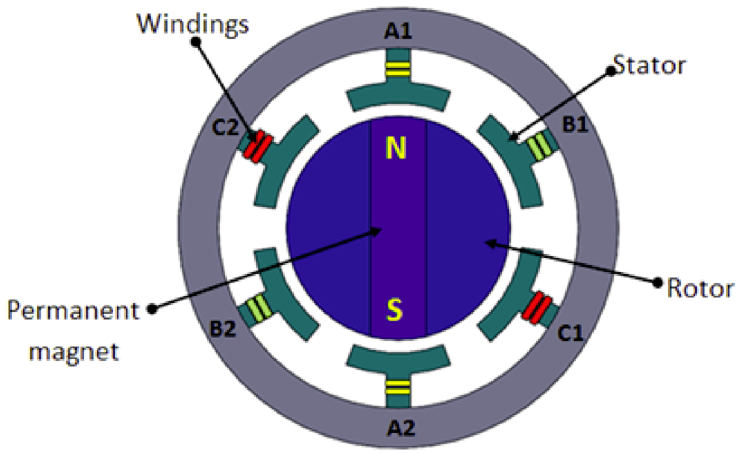

Figure 2.7: BLDC motor [40]

dc voltage across the stator winding's, the coil will energize and become electromagnet. Due to the interaction between the electro-magnet and permanent magnet a electro-motive force is generated which rotates the motor. The Figure 2.7 shows three stator slots and a magnetic pole pair. When coil A is energized, the opposite poles of stator and rotor attracts each other. As the rotor nears coil A, coil B gets energized. As the rotor nears coil B the coil C gets energized. After that coil A is energized with opposite polarity. This process is repeated and the motor is rotated continuously. In this case only one coil is energized at a time. To energize two coils at a time the BLDC motors are connected in star form. This will increase the power generated by the motor. In delta type all the three motors are energized at a time. This will increase overall speed generated by the motor. The cobra motor used for generating the thrust is of delta winding. Higher the RPM, higher the thrust produced in equation 2.1. To energize the coils the position of each coil is important.

2.3.2 Advantages of BLDC motor over DC motors [41]

- Better speed versus torque characteristics
- High dynamic response
- High efficiency
- Long operating life due to a lack of electrical and friction losses
- Higher speed ranges
- No sparking due to absence of brushes
- Responsiveness and quick acceleration due to low rotor inertia

3 A study on Electronic speed controllers for UAV's

The ESC is responsible for controlling the speed of the BLDC motor by using an inverter circuit depending on the received signal from the FC; this is achieved by changing the amount of power to the BLDC motor [42]. The ESC provides a link between the electric motor and the power supply. The goals of this chapter is;

1. *"To study different types of ESC protocols, and the influence of the FC control-loop on these protocols."*
2. *"To select a suitable ESC with embedded current, and angular velocity sensing."*

3.1 ESC protocols

ESCs use different protocols to communicate between the FC; one of its tasks is to receive the throttle signal from the FC [43]. The ESC decodes this signal and controls the speed of the motor. This communication is uni-directional. The protocols can be characterized by their communication speed, pulse length, and analog or digital communication. The different ESC protocols are PWM, Oneshot, dshot, and proshot.

3.1.1 PWM

PWM is an electrical pulse that varies from 0 to 100%; such pulses have a defined interval. The servos use an odd-ball PWM also called PPM signals, where pulses vary from 1000 to 2000μs to communicate. The 0% throttle value is 1000μs and 100% throttle value is 2000μs. Here the position of the pulse encodes the value within the window. The drawback of using PWM signal is;

- The maximum update rate is 500Hz.
- Jitter in the output signal because the output of the FC control-loop is not synced with the PWM signal. The Figure 3.1 shows the comparison of No jitter and real-world condition.

3.1.2 Oneshot

The Oneshot protocol was designed to tackle synchronization and delay issues. This protocol has technical advancement when compared with the PWM signal. It is a combination of two signals, namely, syncPWM and fastPWM. The syncPWM sends the throttle signal to the ESC at the exact time when the FC control-loop finishes it's calculation. The Figure 3.2 shows the sync PWM signal. The fastPWM increases the pulse length, resulting in high update rates. The Oneshot protocols have different PWM pulse length range. The following are the Oneshot protocols distinguished on their pulse length;

- Oneshot125: It has a PWM pulse length of 125 to 250μs, with a maximum update rate of 4kHz.
- Onseshot42: It has a PWM pulse length of 42 to 84μs, with s maximum update rate of 12kHz.
- Multishot: It has a PWM pulse length of 12.5 to 25μs, with a maximum update rate of 40kHz.

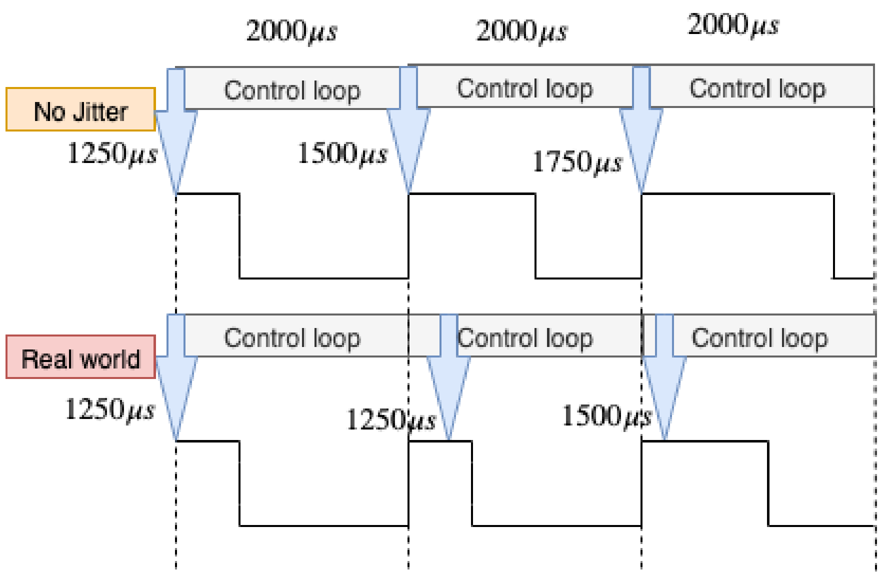

Figure 3.1: PWM signal comparing no jitter and real-world case. Blue arrow is the control-loop signal sent by the FC. At no jitter(or ideal) case, the ESC will receive the same pulse sent by the FC. However, in real-world the control-loop takes time to execute, resulting in a delay, because PWM is not synced it will repeat the previous pulse.

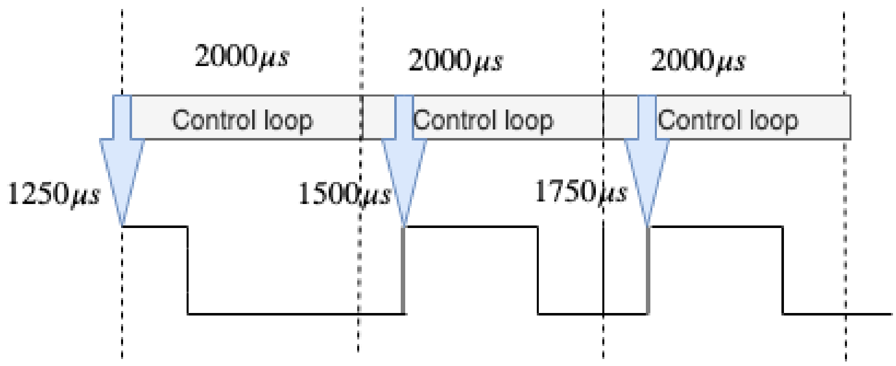

Figure 3.2: SyncPWM signal used by Oneshot ESC. It can be seen that as soon the control-loop executes, the ESC will read the new pulse value updated by the control-loop in FC.

The PWM and the Oneshot are analog protocols and have some issues like,

- They are sensitive to inaccurate calibration. i.e., if the clocks of the analog sensors are not running at the same speed, the value is misread. The calibration is necessary for analog protocols because of oscillator drift.
- Electrical noise in the system limits accuracy in analog signals. The noise will affect short pulse(Oneshot42, multishot, and Oneshot125)more than longer pulses(PWM).

3.1.3 Dshot

To overcome the issue in analog protocols,the digital protocols were invented. The Dshot also referred to as digital shot is a digital protocol used to communicate between FC and ESC. They can operate at high speed. The Dshot protocol uses DMA to send high bit-rate data without overloading the ESC CPU.

Dshot ESC uses ac16-bit data packet. 11-bit for throttle value($2^{11} = 2048 steps$), 1-bit for telemetry and 4-bit for CRC. The CRC will increase the accuracy by detecting errors during communication; then the ESC will reject the corrupted data. The telemetry has sensing option to measure voltage, the temperature of ESC, current and motor angular velocity. Once the ESC receives a high telemetry bit from the FC, ESC transmits back a 10 8-bit byte signal with sensed data to FC. The Figure 3.3 shows the 10 8-bit byte signal. Only current and angular velocity measurement data are used in this research. ESC uses a shunt resistor to measure current by the voltage drop across the resistor, by applying ohms law current drawn by the motor can be obtained. ESC uses a back emf zero-crossing method to measure angular velocity.

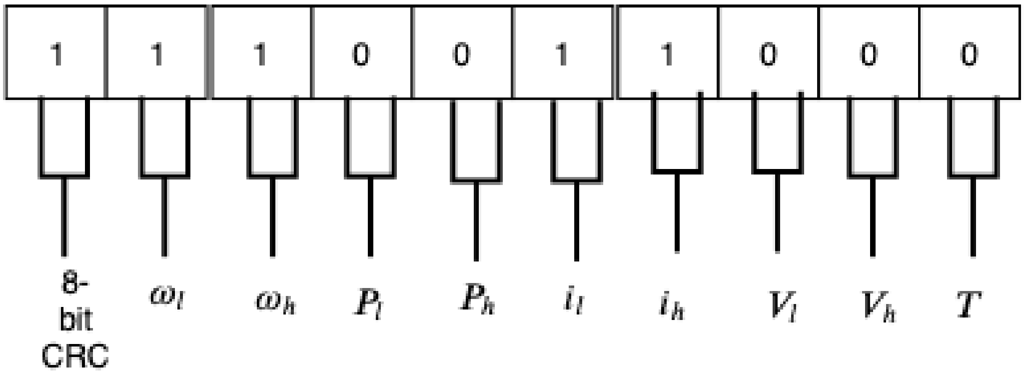

Figure 3.3: 10 8-bit bytes transmission from ESC to FC when the telemetry bit is high. The rightmost bit is the lowest bit and the leftmost is the highest bit. First rightmost bit 'T' is temperature, the v_h, and v_l is voltage high byte and low byte respectively, the i_h, and i_l is current high byte and low byte respectively, the p_h, and p_l is power consumption high byte and low byte respectively, the ω_h, and ω_l is ERPM high byte and low byte respectively, 8-bit CRC byte is the error detecting and rejecting of a corrupted telemetry signal. Current, ERPM, and 8-bit CRC are high for sensing.

The advantages of using Dshot signal is[1];

- No calibration is required.
- It has high resolution of 2048 steps.
- high accuracy signals.
- ESC can detect every signal and reject corrupted data.
- It does not require additional capacitor to filter noise. Resulting in smaller size of the ESC.

Table 3.1: Table for different Dshot protocols

Protocol	data per second(Kpbs)	Maximum update rate(Khz)
Dshot150	150	8
Dshot300	300	16
Dshot600	600	32
Dshot1200	1200	74

[1] https://oscarliang.com/dshot/

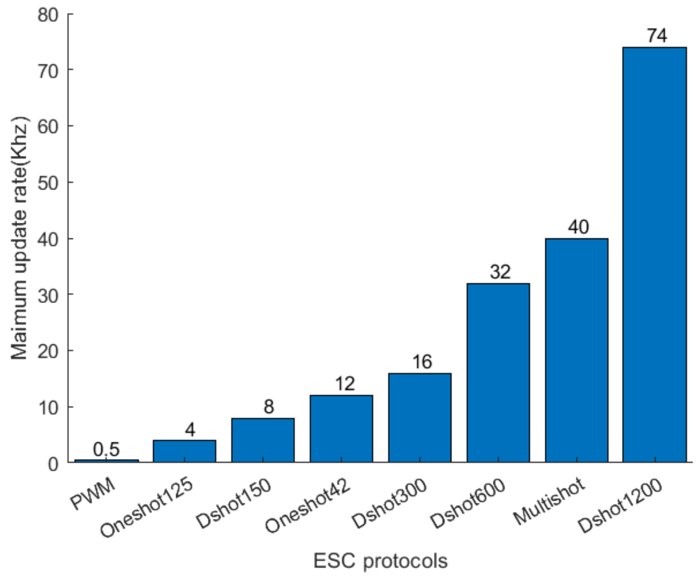

Figure 3.4: ESC frequency comparison at 100% throttle.

3.2 ESC selection

BLheli32 ESC using Dshot protocol has embedded sensing. BLheli32 is firmware designed by BLheli developers, which runs on 32-bit MCU (STM32F0 Cortex-M0 at 48MHz) [44]. In this section, a compression of ESCs is done based on their specifications, and a suitable ESC is chosen.

Table 3.2: Compression table based on ESC specifications

Specification	DYS BLhelis	Lumeniaer BLheli32	Airbot wraith32	kiss32A	Aikon 4in1
PWM	✓	✗	✓	✓	✓
Oneshot125	✓	✓	✓	✓	✓
Oneshot42	✗	✓	✓	✓	✓
Multishot	✗	✓	✓	✓	✓
Dshot	✗	✓	✓	✓	✓
Current Sensor	✗	✓	✓	✓	✓
ω Sensor	✗	✓	✓	✓	✓
Resolution	1000 steps	2048 steps	2048 steps	2048 steps	2048 steps
weight	20g	6g	14g	8g	10g
communication	✗	FTDI and FC and FC	FTDI and FC	FC	FTDI and FC

Table 3.2 shows the comparison of ESCs based on their protocols, telemetry, communication, and resolution. The DYS BLheli ESC is the existing ESC used at the RAM lab for interaction tasks. The choice was made among the other 4 ESCs. The DYS BLheli ESC uses the PWM protocol for communication between EC and ESC, hence the choice was to be made between the ESCs which use the PWM protocol for communication; hence Lumeniaer ESC was left out. The kiss32A ESC needs a FC with DMA to transmit the sensor data, the work in this thesis is the use of BLDC motor to understand the thrust change in the influence of external wind, hence buying a new FC for this purpose was not an option. Aikon 4in1 ESC has embedded 4 ESCs in it, the current sensor used in Aikon ESC will measure the total current drawn by all the ESCs. In case of disturbances acting on a multi-rotor, the thrust produced by each rotor is different, so measuring the overall current does not seem a feasible solution. The Airbot wraith32 ESC is se-

lected for measuring current and rotor angular velocity. This ESC has an inbuilt digital current sensor gives more precise readings and eliminates drift. The sensor data can be received every 32ms.

3.3 Conclusion

- A study on protocols used in ESC was carried out, and it was observed that Dshot1200 protocol has high accuracy, high resolution, do not require calibration, higher speed, and reduced size.
- PWM signal is used for communication between the Arduino and BLDC motor in chapter 4 because already existing hexacopter uses PWM signals for communication between FC and ESC.
- Airbot wraith32 ESC is selected depending on the specification requirement. The requirements where the ESC should have an embedded current and angular velocity sensor and its compatibility with PWM communication.

4 Analyzing influence of wind disturbances on thrust

In this chapter, a detailed study on the effect of disturbances on a single rotor is studied. The ESC Airbot Wraith32 selected from chapter 3 is used to measure the current and angular velocity of the rotor in this chapter. This chapter is divided into four sections; the first section will explain the measurement setup, and the second section will explain the experimental procedure, the third section consists of experimental results, and ending with a conclusion. The goal of this chapter is,

1. *"To observe the effect of disturbances caused by a non-stationary airflow on the rotor. The change in airflow can be due to airflow-blocking objects(floor, wall or the corner of the wall or ground effect) or because of airflow creating objects(another rotor). The observation is made by comparing the thrust, current, rotor angular velocity, and drag torque measurements at different disturbances with the static measurements."*

2. *"To observe the change in current, rotor angular velocity, drag torque due to change in Thrust. The observation is a base to design a suitable estimator in chapter 5."*

4.1 Experimental Setup

This section describes the measurement setup and the equipments that were used to perform the experiments. All the experiments where performed at the flight laboratory in RAM at the University of Twente. The laboratory provides a dedicated area for UAV experiments which is protected by the transparent shield for safe operations. The Figure 4.1 shows the experimental setup used in the lab. An overview of the system used to conduct experiments is shown in the Figure 4.2. The experimental setup includes a BLDC motor, a propeller, a control unit, a driving unit, a measuring unit, and a power supply. All the subsystems are briefly explained below.

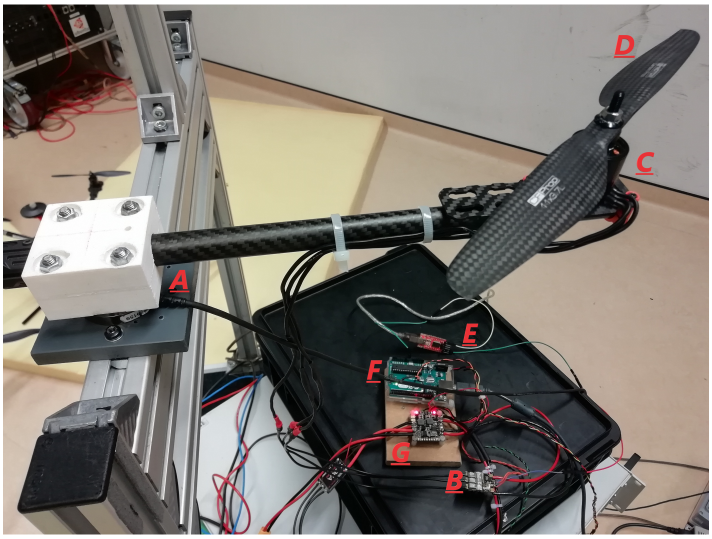

Figure 4.1: Experimental test setup. Where A is Force/torque sensor, B is Airbot Wraith32 ESC, C is Cobra CM2217/20 BLDC motor, D is T-motor $11x3.7$ propeller, E is FTDI and F is Arduino and G is power distribution board.

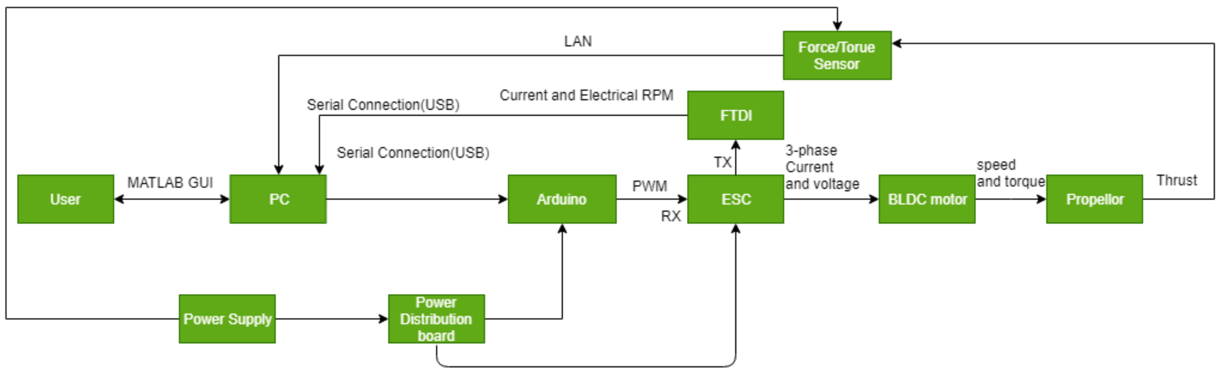

Figure 4.2: Measurement system showing the connections for a single rotor.

4.1.1 BLDC motor and propeller subsystem

The BLDC motor and propeller represents an arm of the hexacopter used in SPECTORS project and were already chosen. The motor used for the experiments is a Cobra CM2217/20 [45], and the propeller is T-motor $11x3.7$ [46]. The choice of propeller and BLDC motor is crucial because it decides the amount of thrust the rotor can generate.

4.1.2 Control Unit

The control unit is a PC, installed with MATLAB to generate motor PWM in percentage using a GUI to make real-time changes and to record the measuring unit data using the data inspector tool in MATLAB Simulink. The PC is connected to the measurement units using USB for serial communication of the telemetry data from the ESC and LAN connection for force and torque sensor. The desired throttle is sent from the control unit to the Arduino UNO [47] through a USB serial communication. For the test in the influence of another rotor, the MATLAB is programmed such that two motors can be controlled at the same time and the block diagram of it is shown in the Figure 4.3.

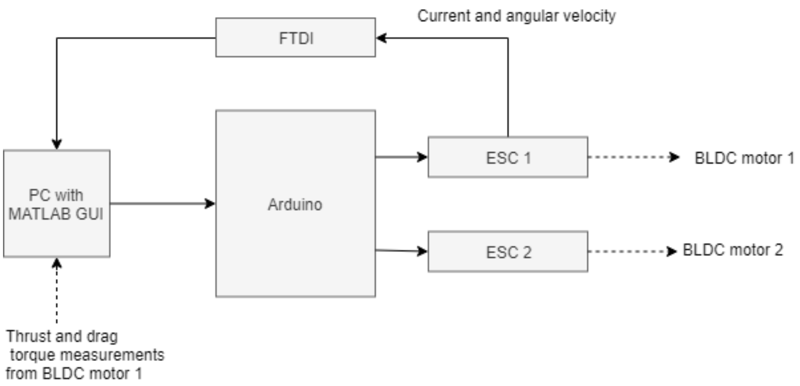

Figure 4.3: MATLAB program enhanced such that it can control two motor's speeds

4.1.3 Driving Unit

The driving unit consists of Arduino UNO has a PWM generator and Airbot Wraith32 to control motor speed. The Arduino receives the PWM signal(throttle) sent by the PC through the serial port. The received data is then transmitted to the ESC to control the speed of the BLDC motor by varying the current.

4.1.4 Measuring Unit

The measuring unit comprises of two parts one to measure force and torque by using the ATI Industrial Automation F/T Mini40E [48], this data is used to design the fitted model and to compare the estimated data in chapter 5. The second part is the ESC which has an embedded current, and angular velocity sensor. The Airbot Wraith32 uses a digital sensor to measure current and direct back emf method to measure rotor angular velocity[1]. The measurements are done at a sampling rate of 1 millisecond.

4.2 Experimental procedure

This section explains the experiments conducted. For clarity, they are separated by different situations namely, situation A testing in the influence of airflow blocking objects and situation B, the influence of another rotor system.

The variables that are changed during the measurements are the motor PWM and the distance between the rotor and the airflow blocking object or in the presence of a disturbing object. The airflow blocking can be due to the wall effect or the corner effect. The disturbing object here is another rotor system. The measured variables are thrust, drag torque, current and the angular velocity of the rotor. A constant voltage of 16 volts is used to conduct the experiments.

The motor duty cycle is increased from 0 to 100%, in a step size of 10% every 25 seconds for all the experiments. Where 0 is when the motor is off, and 100 is at full speed. The thrust, angular velocity, current, and torque are measured at a sampling time of 1ms. The propeller is rotated in a clockwise direction for all the experiments.

At first, a static experiment is conducted. It is carried out by placing the rotor at the center of the room without any disturbances. The test in realistic condition will represent the multi-rotor UAV without any external disturbance. The measurement results obtained from this test are used to compare with the measurements obtained in the presence of disturbance. The Figure 4.4 shows the static test schematic and test setup.

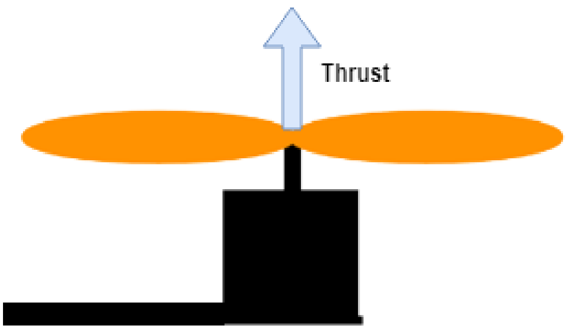

(a) Schematic representation of static test.

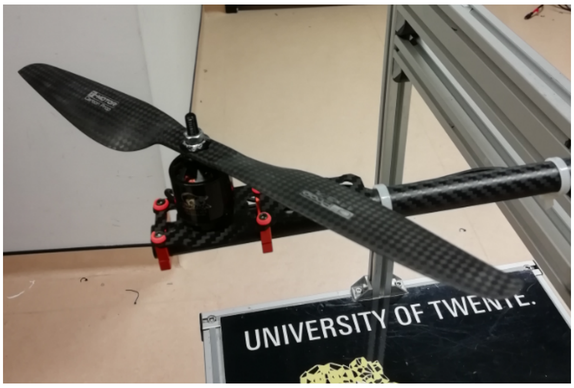

(b) Static test experiment.

Figure 4.4: Static test situation.

The experiments can be distinguished has follows:

1. Test for a single rotor model
    - A1: The rotor is placed at a distance of 2cm from the wall. It shows the effect of an airflow when the rotor is blocked from one side. In a realistic situation, this experiment is a replica of UAV close to the wall. The Figure 4.5 shows the schematic and setup model.

[1] discussed in chapter 2

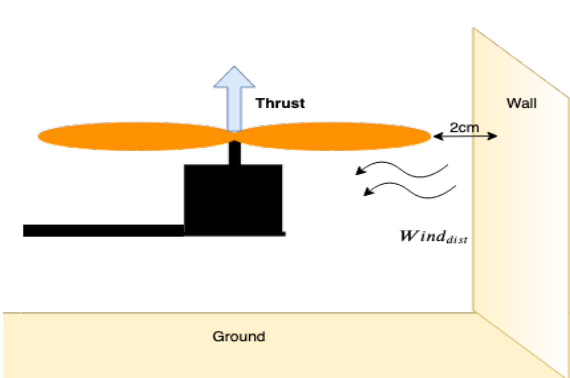

(a) Schematic representation of the rotor near the wall(A1).

(b) Rotor near wall(A1) experiment.

Figure 4.5: Rotor near wall(A1) situation.

- A2: The rotor is placed at a distance of 2cm from each side of the wall near the corner. It shows the effect when the airflow of the rotor is blocked from two sides and is shown in the Figure 4.6. In a realistic situation, this experiment is a replica of UAV close to the corner and in a confined space.

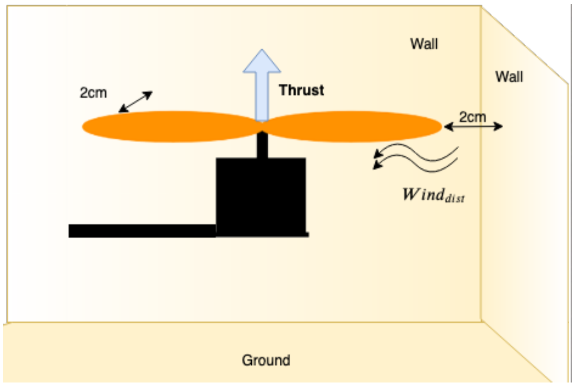

(a) Schematic representation of the rotor near the corner(A2).

(b) Rotor near corner(A2) experiment.

Figure 4.6: Rotor near the corner(A2) situation.

- A3: The rotor is placed at a distance of 20cm above the ground level, the airflow due to the spinning rotor will create a realistic situation where the UAV is close to the floor/ground. The Figure 4.7 shows the schematic and experimental setup.

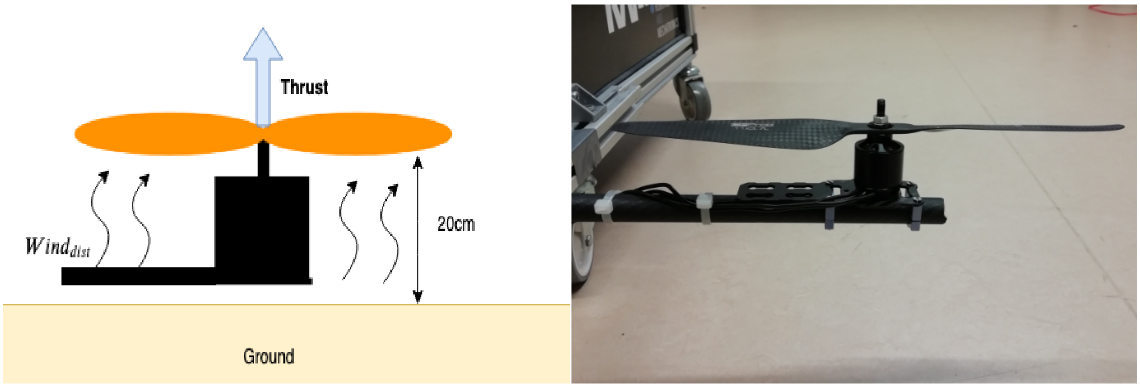

(a) Schematic representation of rotor near ground(A3).

(b) Rotor near ground(A3) experiment.

Figure 4.7: Rotor near ground(A3) situation.

2. Test in the influence of another rotor

   - B1: One rotor to which the sensors are connected is placed similar to the Static test, and the other rotor is placed tilted, as shown in the Figure 4.8. The PWM signal is varied has similar to the static test for both the rotors. For a realistic case this situation is similar to the tilted rotor condition. Both rotors are placed at 15cm in the distance with each other. The tilted rotor is placed at an angle of 47.7°.

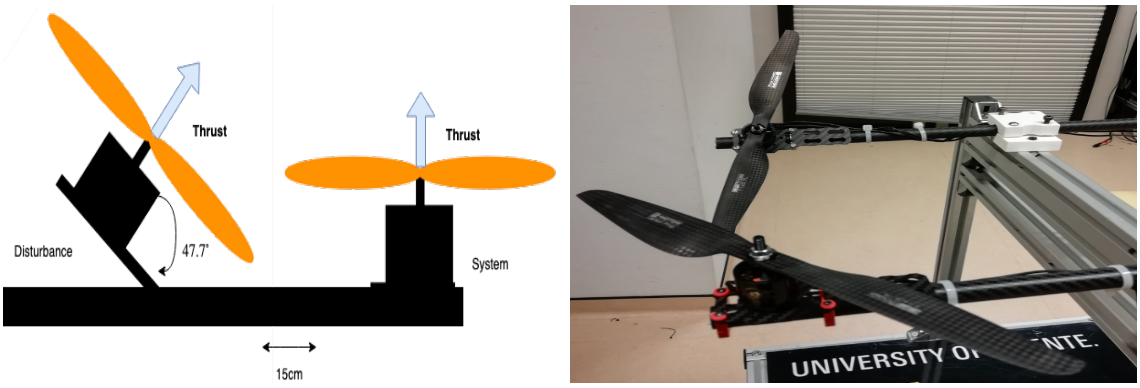

(a) Schematic representation of tilted rotor(B1).

(b) Tilted rotor (B1) experiment.

Figure 4.8: Tilted rotor(B1) situation.

   - B2: This setup is similar to the B1, here the tilted rotor is runs at a constant motor PWM speed of 50%. This is a realistic case when the wind is flowing sideways towards the UAV. Figure 4.8 shows the schematic and test setup as the setup is similar to B1.

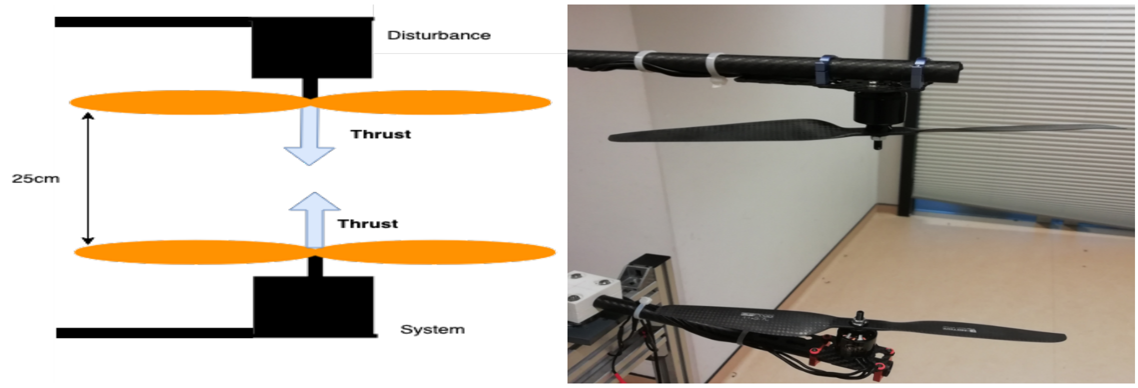

(a) Schematic representation of vertical rotors facing each other(B3).

(b) Vertical rotors are facing each other(B3) experiment.

Figure 4.9: Vertical rotors facing each other(B3) situation.

- B3 and B4: The two rotors are placed vertically, to analyze the upward and downward wind effect. One rotor is run by a constant motor PWM speed of 50%, and PWM of the other rotor is changed between 0 to 100%. The rotor with constant speed is placed at the top rotor facing downwards at a distance of 20cm is B3 experiment; this setup generates downward wind and shown in the Figure 4.9. When the constant running rotor is placed below facing upwards is B4; it will generate upward wind and shown in the Figure 4.10. The motor PWM of the steady rotor is 50% because when hovering in free air, the motors of UAV are spinning around 50%. In both the case B3, and B4 the rotors are placed at 25cm apart, to reduce the factor of upper rotor high pressure on lower rotor a distance of 25cm is maintained throughout the test.

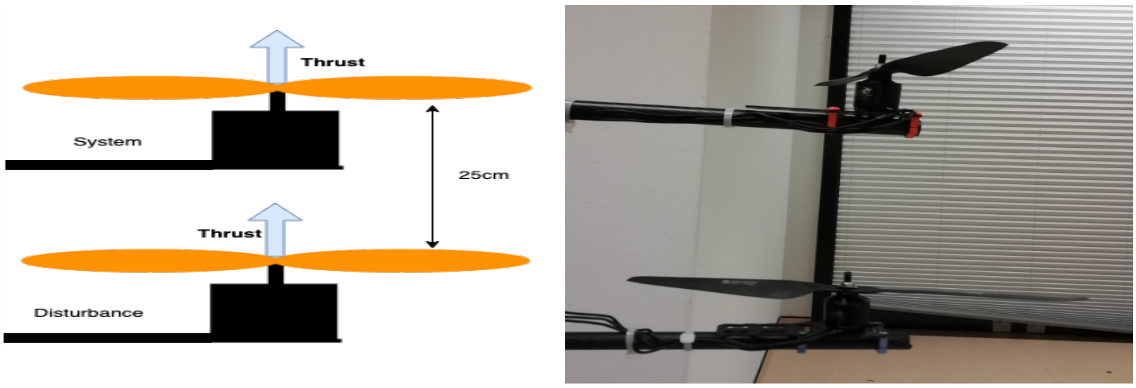

(a) Schematic representation of rotors facing upwards vertically (B4).

(b) A Wind gust of rotors facing upwards vertically(B4) experiment.

Figure 4.10: Wind gust of rotors facing upwards vertically(B4) situation.

- B5: This condition is similar to the B4 situation, but the system and disturbances are interchanged in this case. The disturbance rotor, which is placed at the top is rotated at a constant speed of 50%. The distance between the propellers is 25cm apart.

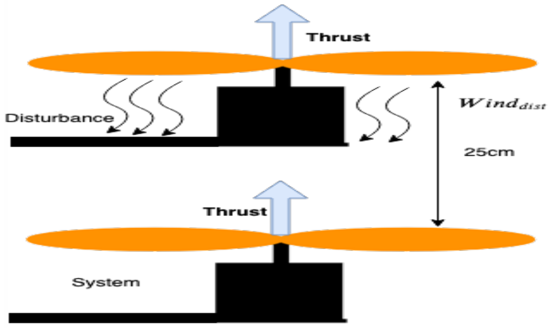

(a) Schematic representation of wind gust downwards(B5).

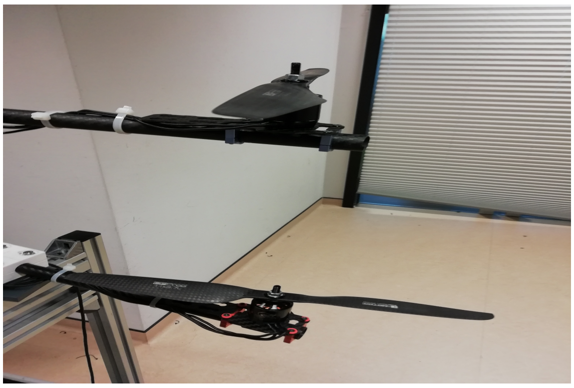

(b) Wind gust upwards(B5) experiment.

Figure 4.11: Wind gust downwards(B5) situation.

The experiments were conducted for different distances from the blocking object. The maximum difference in the static and the measurement influenced by disturbance object was observed at 2cm. Hence all the blocking object measurements were tested at 2cm distance. For safety reasons, while working with two rotor model, they were placed at a distance of 25cm each. For ground effect testing the minimum available distance between the ground and rotor was 25cm due to the experimental setup constrain. The tilted rotor is placed at 15cm apart. All the experiment tests are summarized in Table 4.1 for easy conveying.

Table 4.1: Table summarizing all the experimental test's

Experimental setup situation	Experiment test condition
Static	Test in the absence of disturbances is shown in the Figure 4.4
A1	Rotor near the wall is shown in the Figure 4.5
A2	Rotor near the corner is shown in the Figure 4.6
A3	Ground effect on the rotor is shown in the Figure 4.7
B1	Tilted rotor effect is shown in the Figure 4.8
B2	Wind gust sideways is shown in the Figure 4.8
B3	Wind gust downwards shown in the Figure 4.9
B4	Wind gust due to rotors facing upwards vertically is shown in the Figure 4.10
B5	Wind gust from motor placed above vertically is shown in the Figure 4.11

4.3 Experimental measurements and analysis

This section contains the results and evaluation of the experimental tests. The measurement data obtained from each of the tests is filtered by taking the mean and standard deviation in MATLAB and this filtered data are analyzed by comparing the data with the static measurement filtered data. Listing each plot for a single experiment consumes a lot of space; hence, each situation i.e., air blocking and air generating rotor is compared with the static case in individual plots. This section consists of four subsections analyzing experimental data of thrust, drag torque, current, and rotor angular velocity.

4.3.1 Thrust measurement at different experimental situation

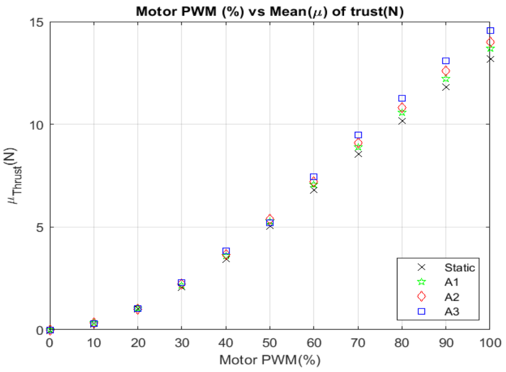

(a) Motor PWM speed vs mean thrust at static experiment and experiment test situation A.

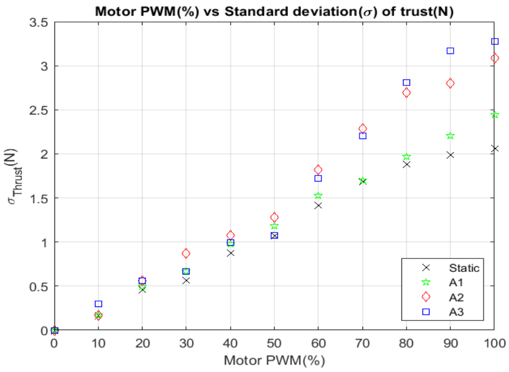

(b) Motor PWM speed vs standard deviation of thrust at static experiment and the experiment test situation A.

Figure 4.12: Motor PWM speed vs filtered thrust at static experiment and experiment test A situation. The μ and σ are the symbol for mean and standard deviation respectively. Table 4.1 shows the summary of experiment situation A.

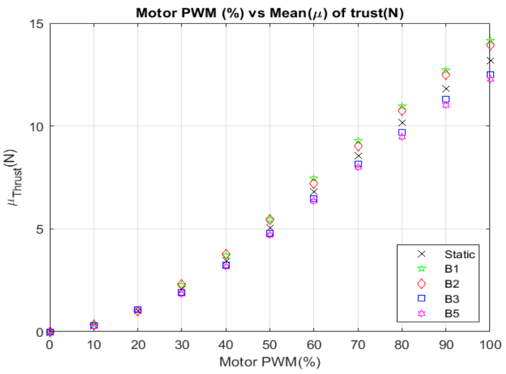

(a) Motor PWM speed vs mean thrust at static experiment and experiment test situation B.

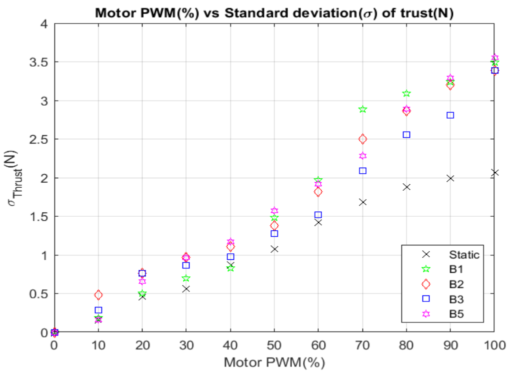

(b) Motor PWM speed vs standard deviation of thrust at static experiment and experiment test situation B.

Figure 4.13: Motor PWM speed vs filtered thrust at static experiment and experiment B test situation. The μ and σ are the symbol for mean and standard deviation respectively. Table 4.1 shows the summary of experiment situation B.

Table 4.2: Comparison of mean static condition thrust data with different experimental test condition mean thrust data for motor PWM ranging between 0 to 100 %. The table shows the error between test situation and static method, i.e . $E_{(A2)} = E_{(A2-static)}$. The color code in the table shows lowest↑ , highest↑ for experiments whose thrust change is positive, lowest↓ and highest↓ for experiments whose thrust change is negative. Table 4.1 shows the summary of all experiment situation.

PWM	$E_{(A1)}$	$E_{(A2)}$	$E_{(A3)}$	$E_{(B1)}$	$E_{(B2)}$	$E_{(B3)}$	$E_{(B5)}$
0	0	0	0	0	0	0	0
10	0.0120	0.0188	0.0025↑	0.0224	0.0273↑	-0.0158↓	-0.0312↓
20	-0.0010↑	-0.0044	-0.0013	-0.0165	-0.0592↑	0.0020↓	0.0108↓
30	0.0802↑	0.1377	0.2006	0.1616	0.2074↑	-0.1870↓	-0.2437↓
40	0.1348↑	0.2120	0.3660↑	0.2517	0.2950	-0.2177↓	-0.3586↓
50	0.1878	0.3110	0.1373↑	0.3903↑	0.3801	-0.2879↓	-0.4109↓
60	0.2600↑	0.3978	0.6218↑	0.6361	0.3943	-0.3503↓	-0.4402↓
70	0.3340↑	0.5449	0.9059↑	0.6884	0.4629	-0.4202↓	-0.5709↓
80	0.3971↑	0.6242	1.0784↑	0.7613	0.5642	-0.5001↓	-0.6926↓
90	0.3991↑	0.7841	1.2521↑	0.8907	0.6867	-0.5277↓	-0.8158↓
100	0.5141↑	0.8080	1.3959↑	0.9596	0.7433	-0.6775↓	-0.9095↓

The Figure 4.12, The Figure 4.13 shows the mean and standard deviation of motor PWM vs. thrust at A situation and B situation, respectively. Table 4.2 shows the change in thrust in A and B situation when compared with static situation test. The reason for the change in thrust could be summarized as;

- Change in AOA due to additional wind created by blocking objects or an air-flow creating object.
- Change in streamline wind velocity.
- Less effect of tip vortex on the propeller because of the wall or other rotors, increasing of thrust.
- High measurement noise is observed. It is because of wind disturbances acting on the propeller; this disturbances are due to air-flow blocking or air-flow creating object. Figure 4.12b and Figure 4.13b shows the standard deviation of the experimental measurements. Higher the standard deviation higher noise is observed during experiments.

1. A1 situation:
    - Table 4.2 shows a minimum change in thrust when compared at all the situations where the disturbance creates positive change in thrust. A mean thrust error of 3.69% increase is seen in the A1 situation.
    - The lowest thrust error is 0.09512%decrease is observed at 20% motor speed, and the highest error of a 3.89%increase is observed at 100% motor speed. A mean thrust error of a 3.69% increase is seen at the A1 situation.
    - The reason for thrust change is, the wall blocks the tip vortex air-flow, which then increases the pressure beneath the propeller. i.e., the up-flow wind is more, in this case, will increase the thrust. The increasing measurement noise is shown in Figure 4.12b. Comparatively the noise is less at this situation when compared with other test situations.

- The change in thrust, when placed near the wall can be neglected because the interacting UAVs use a manipulator for contact purposes which results in creating a distance more than 10cm between the wall and propeller end. Figure 1.1a shows the multi-rotor UAV with a manipulator.

2. A2 situation:

   - The lowest thrust error is 0.4185%decrease is observed at 20% motor speed, and the highest error of 6.12%increase is observed at 100% motor speed. A mean thrust error of a 6.07% increase is seen at the A1 situation.
   - Similar to the A1 situation, the tip vortex and air trapping beneath the propeller will increase thrust. Figure 4.12b shows the measurement noise increase due to the disturbance created by air-blocking on both sides of the rotor. The measurements showed high noise at higher motor speed,i.e., motor speed between 60% to 100% has high noise.
   - The change in thrust cannot be neglected when a multi-rotor UAV is in confined space where one or more rotors are surrounded by blocking(wall) object because of lesser space for the air to circulate, creating higher thrust and noisy measurements.

3. A3 situation:

   - A maximum thrust is observed at the A3 situation while comparing it with other situations which has a positive error in thrust.
   - The lowest thrust error is 0.1235%decrease is observed at 20% motor speed, and the highest error of 10.58%increase is observed at 100% motor speed. A mean thrust error of a 9.51% increase is seen at the A3 situation.
   - The reason for the change in thrust is smaller the distance between the propeller and the ground; more air gets trapped, generating high pressure beneath propeller increasing in thrust produced. Figure 4.12b shows high noise in the thrust measurement. High variance is observed at A3 condition than other experimental situations.
   - The multi-rotors, in general, have legs to stand on the ground, creating a certain distance between the ground and the propeller. Thus, the UAV stand height influence on the thrust change. The A3 condition makes the takeoff and landing of multi-rotors difficult.

4. B1 situation:

   - The lowest thrust error is a 1.56%decrease is observed at 20% motor speed, and the highest error of a 7.27%increase is observed at 100% motor speed. A mean thrust error of a 7.61% increase is seen at the B1 situation.
   - The possible reason for thrust increase would be because the tilted rotor sucks the vortex air-flow, creating high pressure beneath the rotor whose thrust is measured. The measured thrust as high noise visible from Figure 4.13b.
   - For motor speed between 50 to 100% the thrust measurement shows very high noise. This is because of the influence of other rotor suystem.
   - The B1 situation is for the UAV which is fully-actuated, the effect of the propeller facing each other cannot be neglected, because of this influence instability in flight.

5. B2 situation:

   - The lowest thrust error is 5.21%decrease is observed at 20% motor speed, and the highest error of a 9.96%increase is observed at 30% motor speed. A mean thrust error of a 5.92% increase is seen at the B2 situation.

- A high thrust change is observed between 10%, 30%, and 40% because of the tilted rotor creating the gust flow rotates at a constant speed of 50%. The possible reason for thrust increase would be because the tilted rotor sucks the vortex air-flow, creating high pressure beneath the rotor whose thrust is measured. This is similar to B1 condition, but initially a large change is visible because of the constant rotation of the tilted rotor. Also, due to the higher air-flow, the standard deviation of thrust is high between 10% to 40% can be seen in Figure 4.13b.
- The effect of gust cannot be neglected when the UAV fly in free air, and there is a sudden gust flow in sideways.

6. B3 situation:
   - This error is lowest while comparing to the situation where the thrust change is negative. Table 4.2 shows a decrease in thrust due to wind disturbance.
   - The lowest thrust error is 0.19%increase is observed at 20% motor speed, and the highest error of 6.29%decrease is observed at 40% motor speed. A mean thrust error of a 5.08% decrease is seen at the B3 situation.
   - The decrease in thrust is due to both the propellers facing each other sucks the air-flow creating a lesser streamflow of wind for both the propellers. The measurement as high noise between motor speed of 60 to 100%, this is because of the external rotor creating high noise.
7. B4 situation:
   - The lower motor at this condition is rotated at 50% motor speed.
   - In this situation, there is a negligible difference in thrust on the upper motor when compared with static measurements, and the difference is shown in Table 4.3. This is because of the upper propeller beneath as high air pressure flowing downward on the lower motor, thus the disturbing lower motor as no influence on thrust change on the upper motor.
   - Due to negligible thrust change, this method is not used for further analysis.
8. B5 situation:
   - The lowest thrust error is 1.02%increase is observed at 20% motor speed, and the highest error of 10.28%decrease is observed at 40% motor speed. A mean thrust error of a 7.14% decrease is seen at the B5 situation.
   - Due to the upper rotor running at a constant speed of 50%, the thrust error decrease is highest when the lower motor rotates at 10%, 30%, and 40%.
   - The error is highest while comparing to the situation where the thrust change is negative. Table 4.2 shows decreasing in thrust due to wind disturbance.
   - The reason for the decrease in thrust is the air-flow of the upper motor pushes air onto the lower one, this results in high-pressure air building up above the lower rotor, resulting in a decrease of pressure difference above and below the propeller. The highest measurement noise is between 60 to 100% motor speed.

Table 4.3: Comparison of mean static condition thrust data with B4 experimental test condition mean thrust for motor PWM speed ranging between 0 to 100%. The table shows the error between B4 and static measurement test. The color code in the table shows lowest and highest thrust values.

PWM	Static thrust	B4 thrust	$E_{(B4-Static)}$
0	0	0	0
10	0.3078	0.3068	-0.0010
20	1.0513	1.0533	0.0020
30	2.0832	2.0812	-0.0020
40	3.4586	3.4552	-0.0034
50	5.0739	5.0744	0.0005
60	6.8159	6.8158	-0.0001
70	8.5644	8.5637	-0.0007
80	10.1833	10.1783	-0.0050
90	11.8239	11.8235	-0.0004
100	13.1821	13.1816	-0.0005

4.3.2 Drag torque measurement at different experimental situations

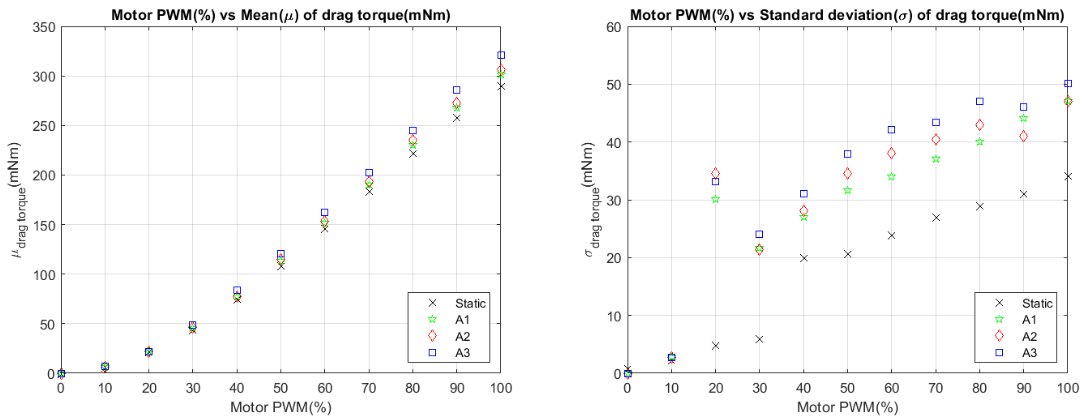

(a) Motor PWM speed vs mean drag torque at static experiment and experiment A test situation.

(b) Motor PWM speed vs standard deviation drag torque at static experiment and experiment A test situation.

Figure 4.14: Motor PWM speed vs filtered drag torque at static experiment and experiment A tests situation. The μ and σ are the symbol for mean and standard deviation respectively. Table 4.1 shows the summary of experiment situation A.

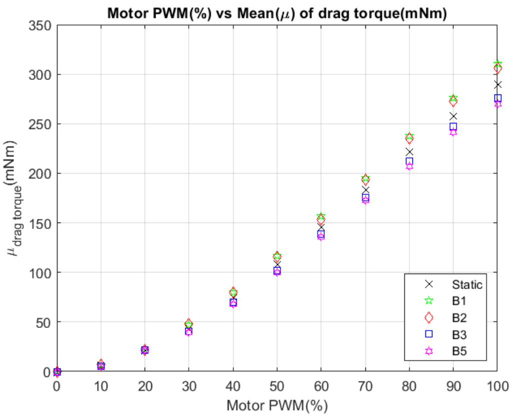

(a) Motor PWM speed vs mean drag torque at static experiment and experiment B test situation.

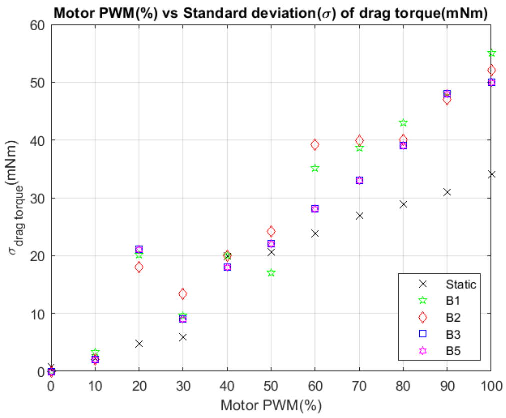

(b) Motor PWM speed vs standard deviation drag torque at static experiment and experiment B test situation.

Figure 4.15: Motor PWM speed vs filtered drag torque at static experiment and experiment B test situation. The μ and σ are the symbol for mean and standard deviation respectively. Table 4.1 shows the summary of experiment situation B.

Table 4.4: Comparison of mean static condition drag torque data with different experimental test condition mean drag torque data for motor PWM ranging between 0 to 100 %. The table shows the error between test situation and static method, i.e . $E_{(A2)} = E_{(A2-static)} \times 10^{-3}$. The color code in the table shows lowest↑ , highest↑ for experiments whose drag torque change is positive, lowest↓ and highest↓ for experiments whose drag torque change is negative. Table 4.1 shows the summary of experiment situations.

PWM	$E_{(A1)}$	$E_{(A2)}$	$E_{(A3)}$	$E_{(B1)}$	$E_{(B2)}$	$E_{(B3)}$	$E_{(B5)}$
0	0	0	0	0	0	0	0
10	0.2262	0.0943↑	0.6059↑	0.3219	0.5424	-0.4057↓	-0.6219↓
20	-0.0149	-0.0065↑	-0.0552	-0.0784	-0.2254↑	0.0941↓	0.1093↓
30	1.4277↑	2.2460	4.3972↑	2.9852	3.7892	-3.1996↓	-4.0355↓
40	2.6271	2.5490↑	8.9521↑	5.0652	5.5631	-4.9272↓	-6.2435↓
50	4.2741↑	6.1926	11.5739↑	7.3964	7.3850	-6.4321↓	-8.3964↓
60	5.8291↑	7.8027	16.9370↑	10.9063	7.8940	-6.9831↓	-9.2683↓
70	6.9362↑	8.9500	19.3193↑	12.0763	9.8754	-8.1667↓	-10.2501↓
80	7.9453↑	12.6559	22.5220↑	14.8739	12.4505	-10.1166↓	-15.3409↓
90	9.2714↑	14.8361	27.8051↑	18.0160	14.3978	-11.2098↓	-16.8156↓
100	10.9823↑	16.5293	30.6808↑	20.0092	16.2394	-14.2994↓	-20.0090↓

The Figure 4.14 and The Figure 4.15 shows the mean and standard deviation of drag torque for all the situations except for B4. The B4 is not considered because it had the lowest change in drag torque value. Table 4.4 shows the error in drag torque while compared with the static test results; the table is divided into two sections one for the positive increase in error and the other with the negative increase.The standard deviation is high for drag torque measurement; this indicates the data points are spread over a broader range of values. *"Note, all the drag torque errors are in* 10^{-3}*, i.e is* $E_{(situation)} = E_{(situation-static)} \times 10^{-3}$*"*. The reason for the drag torque change is,

- external wind flow on the propeller will create a drag force on the propeller, resulting in varying drag torque, this change could be positive or negative depending on the wind streamflow.
- The change drag force leads to a change in thrust produced.
- Less effect of tip vortex on the propeller because of the wall or other rotors; this results an increase in drag force.

The reason for drag torque change is similar to the thrust change, hence at each of the situation, the reason for the drag torque is not discussed again to avoid repetitive reasoning. Only the highest and lowest error change in drag torque is discussed.

1. A1 situation:
   - The lowest drag torque error is 0.06824%decrease is observed at 20% motor speed, and the highest error of 3.785%increase is observed at 100% motor speed. A mean drag torque error of a 3.6% increase is seen at the A1 situation.
   - The percentage error in drag torque value is small compared to the thrust change. This is due to the high nosier signal of drag torque.
   - The A1 situation as the lowest error in drag torque measurement when compared with other situations which as a positive increase trend in drag torque and can be seen from Table 4.4. This trend is similar to the thrust measurement.
2. A2 situation:
   - The lowest drag torque error is 0.029%decrease is observed at 20% motor speed, and the highest error of 5.69%increase is observed at 100% motor speed. A mean drag torque error of a 5.38% increase is seen at the A2 situation.
3. A3 situation:
   - The lowest drag torque error is 0.2528%decrease is observed at 20% motor speed, and the highest error of 12.07%increase is observed at 40% motor speed. A mean drag torque error of of 10.53% increase is seen at the A3 situation.
   - As observed in thrust measurement highest effect of wind disturbance is observed at A3 situation when compared with other situations which as positive drag torque is shown in Table 4.4.
4. B1 situation:
   - The lowest drag torque error is 0.3590%decrease is observed at 20% motor speed, and the highest error of 6.89%increase is observed at 100% motor speed. A mean drag torque error of a 6.77% increase is seen at the B1 situation.
5. B2 situation:
   - The lowest drag torque error is 1.032%decrease is observed at 20% motor speed, and the highest error of 8.870%increase is observed at 10% motor speed. A mean drag torque error of a 5.75% increase is seen at the B2 situation.
6. B3 situation:
   - The lowest drag torque error is 0.4309%increase is observed at 20% motor speed, and the highest error of 6.61%decrease is observed at 40% motor speed. A mean drag torque error of a 4.85% decrease is seen at the B3 situation.

- Due to wind disturbance by B3 situation the lowest error in drag torque is observed when compared with negative drag torque condition, i.e., is B5 situation, this change can be observed from Table 4.4

7. B5 situation:

   - The lowest drag torque error is 0.5005%increase is observed at 20% motor speed, and the highest error of 8.37%decrease is observed at 40% motor speed. A mean drag torque error of a 6.71% decrease is seen at the B5 situation.

4.3.3 Motor current measurement at different experimental situation

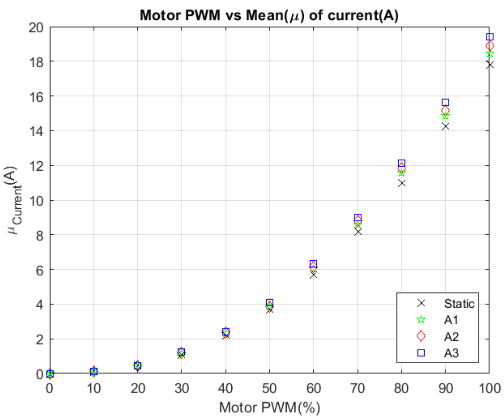

(a) Motor PWM speed vs mean motor current at static experiment and experiment test A situation.

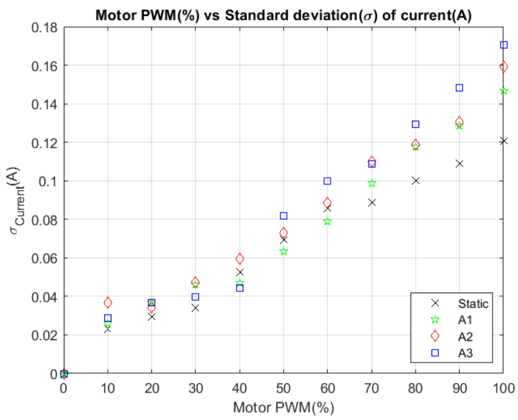

(b) Motor PWM speed vs standard deviation motor current at static experiment and experiment test A situation.

Figure 4.16: Motor PWM speed vs filtered motor current at static experiment and experiment test A situation. The μ and σ are the symbol for mean and standard deviation respectively. Table 4.1 shows the summary of experiment situation A.

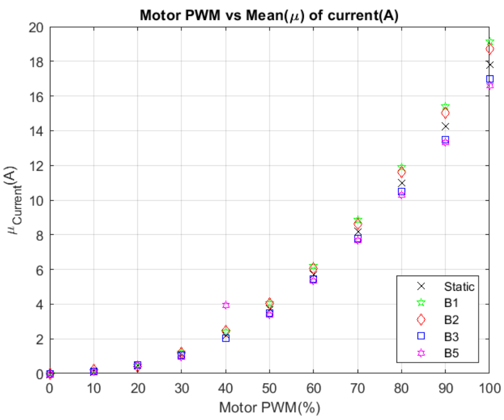

(a) Motor PWM speed vs mean motor current at static experiment and experiment test situation B.

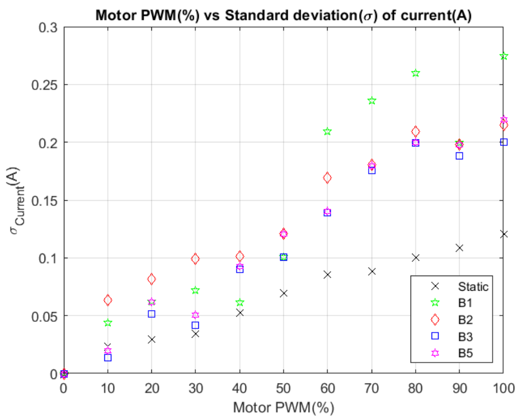

(b) Motor PWM speed vs standard deviation motor current at static experiment and experiment test situation B.

Figure 4.17: Motor PWM speed vs filtered motor current at static experiment and experiment test situation B. The μ and σ are the symbol for mean and standard deviation respectively. Table 4.1 shows the summary of experiment situation B.

Table 4.5: Comparison of mean static condition motor current data with different experimental test condition mean motor current data for motor PWM ranging between 0 to 100 %. The table shows the error between test situation and static method, i.e . $E_{(A2)} = E_{(A2-static)}$. The color code in the table shows lowest↑ , highest↑ for experiments whose current change is positive, lowest↓ and highest↓ for experiments whose current change is negative. Table 4.1 shows the summary of experiment situations.

PWM	$E_{(A1)}$	$E_{(A2)}$	$E_{(A3)}$	$E_{(B1)}$	$E_{(B2)}$	$E_{(B3)}$	$E_{(B5)}$
0	0	0	0	0	0	0	0
10	0.0051	0.0092	0.0042↑	0.0096	0.0690↑	-0.0089↓	-0.0080↓
20	-0.0072	-0.0059	-0.0007↑	-0.0008	-0.0087↑	0.0033↓	0.0013↓
30	0.0309↑	0.0851	0.1105	.0895	0.2041↑	-0.0723↓	- 0.1270↓
40	0.0912↑	0.1699	0.2127	0.1788	0.2396↑	-0.1803↓	-0.2479↓
50	0.1468	0.1303↑	0.3719↑	0.3012	0.3257	-0.2559↓	-0.3491↓
60	0.2603↑	0.3875	0.5735↑	0.4635	0.3226	-0.2967↓	-0.3842↓
70	0.3889↑	0.6104	0.8287↑	0.6631	0.4448	-0.4093↓	-0.4785↓
80	0.5390↑	0.9471	1.1007↑	0.8915	0.6084	-0.5303↓	-0.7174↓
90	0.5783↑	1.1578	1.4857↑	1.1548	0.7669	-0.7669↓	-0.8952↓
100	0.6391↑	1.2787	1.5814↑	1.3429	1.0332	-0.8460↓	-1.10355↓

The Figure 4.16 and The Figure 4.17 shows the mean and standard deviation of motor speed Vs. motor current at A and B situations, respectively. Table 4.5 shows the change in current observed for each situation when compared with the static condition. The standard deviation of the current measurement is low as, shown in Figure 4.16b and Figure 4.17b. Hence it can be concluded that the data points are close to mean value. The reason for the change is;

- The torque generated by the motor is proportional to the current drawn; hence, any change in torque will change the current. For example, an increase in drag torque will increase in current drawn by the motor from rotor-motor equation.

The reason for the current error is similar to the thrust change, hence at each of the situation, the reason for the current change is not discussed again to avoid repetitive reasoning. Only the highest and lowest error change in current is discussed.

1. A1 situation:
   - The error between the A1 and static measurement is low among all the other situations that have an upward trend in current is clearly visible from Table 4.5. It can be concluded that at the A1 situation, the wind disturbance as less effect on the current measurement.
   - The lowest current error is 1.54%decrease is observed at 20% motor speed, and the highest error of 3.9%increase is observed at 80% motor speed. A mean current error of a 3.23% increase is seen at the A1 situation.
2. A2 situation:
   - The lowest current error is 1.06%decrease is observed at 20% motor speed, and the highest error of 6.01%increase is observed at 80% motor speed. A mean current error of a 5.54% increase is seen at the A2 situation.
3. A3 situation:

- The lowest current error is 0.1497%decrease is observed at 20% motor speed, and the highest error of 10.23%increase is observed at 100% motor speed. A mean current error of a 9.06% increase is seen at the A3 situation.
- The error between the A3 and static measurement is high among all the other situations that have an upward trend in current and is clearly visible from Table 4.5. It can be concluded that at the A3 situation, the wind disturbance as high effect on the current measurement for positive trend data.

4. B1 situation:
   - The lowest current error is 0.1711%decrease is observed at 20% motor speed, and the highest error of 7.09%increase is observed at 100% motor speed. A mean current error of a 6.14% increase is seen at the B1 situation.
5. B2 situation:
   - The lowest current error is 1.86%decrease is observed at 20% motor speed, and the highest error of 9.05%increase is observed at 40% motor speed. A mean current error of a 5.42% increase is seen at the B2 situation.
6. B3 situation:
   - The lowest current error is 0.706%increase is observed at 20% motor speed, and the highest error of 6.169%decrease is observed at 40% motor speed. A mean current error of a 4.19% decrease is seen at the B3 situation.
   - The error between the B3 and static measurement is low when compared with B5 which is clearly visible from Table 4.5. It can be concluded that at B3 situation the wind disturbance as low effect on the current measurement for negative trend data.
7. B5 situation:
   - The lowest current error is 0.278%increase is observed at 20% motor speed, and the highest error of 9.52%decrease is observed at 40% motor speed. A mean current error of a 6.19% decrease is seen at the B5 situation.
   - The error between the B5 and static measurement is high when compared with B3, which is clearly visible from Table 4.5. It can be concluded that at the B5 situation the wind disturbance as a high effect on the current measurement for negative trend data.

4.3.4 Rotor angular velocity measurement at different experimental situation

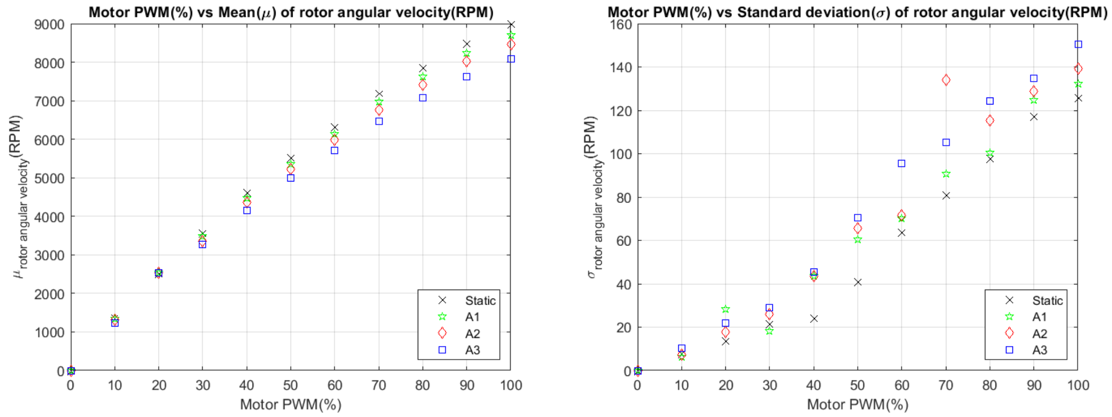

(a) Motor PWM speed vs avearge rotor angular velocity at static experiment and experiment test A situation.

(b) Motor PWM speed vs standard deviation rotor angular velocity at static experiment and experiment test A situation.

Figure 4.18: Motor PWM speed vs filtered rotor angular velocity at static experiment and experiment test A situation. The μ and σ are the symbol for mean and standard deviation respectively. Table 4.1 shows the summary of experiment situation A.

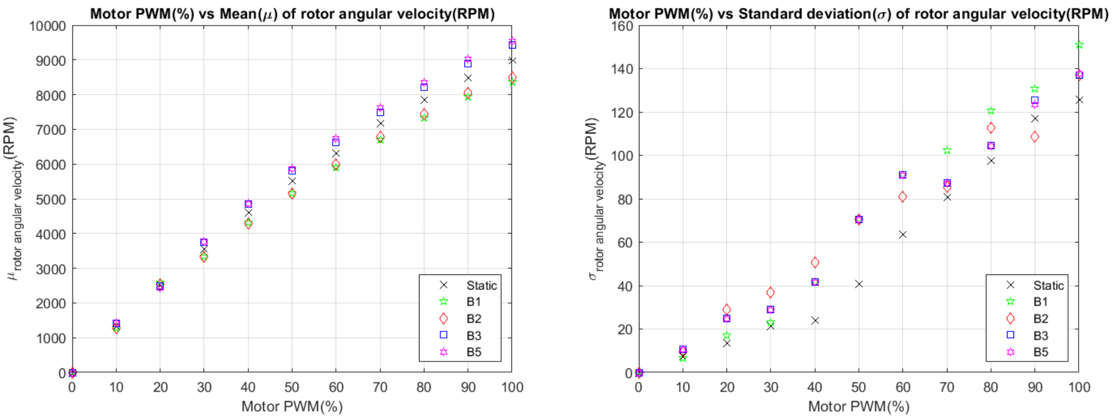

(a) Motor PWM speed vs mean rotor angular velocity at static experiment and experiment test B situation.

(b) Motor PWM speed vs standard deviation rotor angular velocity at static experiment and experiment test situation B.

Figure 4.19: Motor PWM speed vs filtered rotor angular velocity at static experiment and all B experiment tests. The μ and σ are the symbol for mean and standard deviation respectively. Table 4.1 shows the summary of experiment situation B.

Table 4.6: Comparison of mean static condition rotor angular velocity data with different experimental test condition mean rotor angular velocity data for motor PWM ranging between 0 to 100 %. The table shows the error between test situation and static method, i.e . $E_{(A2)} = E_{(A2-static)}$. The color code in the table shows lowest↑ , highest↑ for experiments whose rotor angular velocity change is positive, lowest↓ and highest↓ for experiments whose rotor angular velocity change is negative. Table 4.1 shows the summary of experiment situation's.

PWM	$E_{(A1)}$	$E_{(A2)}$	$E_{(A3)}$	$E_{(B1)}$	$E_{(B2)}$	$E_{(B3)}$	$E_{(B5)}$
0	0	0	0	0	0	0	0
10	-18.2↑	-30.4	-101.3↑	-72.1	-72.9	73.6↓	95.5
20	14.6	22.5	6.8↑	26.4↑	15.7	-42.9↓	-59.6
30	-90.2↑	-210.6	-310.4↑	-237.2	-244.3	169.7↓	215.3↓
40	-148.2↑	-239.4	-446.2↑	-304.7	-325.0	230.5↓	289.8↓
50	-178.2↑	-298.4	-523.5↑	-374.5	-369.21	273.2↓	360.7↓
60	-200.4↑	-350.1	-616.0↑	-426.8	-336.0	294.6↓	382.6↓
70	-215.3↑	-421.4	-706.4↑	-487.2	-383.2	320.1↓	440.1↓
80	-247.0↑	-460.6	-778.3↑	-530.2	-426.9	350.5↓	500.6↓
90	-272.4↑	-482.1	-871.4↑	-570.9	-457.2	400.4↓	537.4↓
100	-302.1↑	-532.3	-899.2↑	-635.3	-502.6	435.0↓	564.3↓

The Figure 4.18 and The Figure 4.19 shows the mean and standard deviation of motor speed Vs. rotor angular velocity at A and B situations, respectively. Table 4.6 shows the change in rotor angular velocity observed for each situation when compared with the static condition. The reason for the change in rotor angular velocity is;

- The torque and motor angular velocity are inversely propositional, i.e., for example increase in drag torque will decrease rotor angular velocity. This results in a decrease in rotor angular velocity when drag torque increases because of the disturbances.

1. A1 situation:
   - The error between the A1 and static measurement is low among all the other situations that have an upward trend in motor angular velocity is clearly visible from Table 4.6. It can be concluded that at the A1 situation, the wind disturbance as less effect on the motor angular velocity measurement.
   - The lowest rotor angular velocity error is 0.579%increase is observed at 20% motor speed, and the highest error of 3.36%decrease is observed at 100% motor speed. A mean rotor angular velocity error of a 2.94% decrease is seen at the A1 situation.
2. A2 situation:
   - The lowest rotor angular velocity error is 0.89%increase is observed at 20% motor speed, and the highest error of 5.918%decrease is observed at 100% motor speed. A mean rotor angular velocity error of a 5.32% decrease is seen at the A2 situation.
3. A3 situation:
   - The lowest rotor angular velocity error is 0.26%increase is observed at 20% motor speed, and the highest error of 10%decrease is observed at 100% motor speed. A mean rotor angular velocity error of 9.34% decrease is seen at the A3 situation.
   - The error between the A3 and static measurement is high among all the other situations that have an upward trend in motor angular velocity and is visible from Table

4.6. It can be concluded that at the A3 situation, the wind disturbance as a high effect on the motor angular velocity measurement for positive trend data.

4. B1 situation:

   - The lowest rotor angular velocity error is 1.04%increase is observed at 20% motor speed, and the highest error of 7.06%decrease is observed at 100% motor speed. A mean rotor angular velocity error of a 6.23% decrease is seen at the B1 situation.

5. B2 situation:

   - The lowest rotor angular velocity error is 0.622%increase is observed at 20% motor speed, and the highest error of 6.55%decrease is observed at 40% motor speed. A mean rotor angular velocity error of a 5.5% decrease is seen at the B2 situation.

6. B3 situation:

   - The lowest rotor angular velocity error is 1.7%decrease is observed at 20% motor speed, and the highest error of 5.05%increase is observed at 40% motor speed. A mean rotor angular velocity error of a 4.4% increase is seen at the B3 situation.
   - The error between the B3 and static measurement is low when compared with the B5, which is clearly visible from Table 4.6. It can be concluded that at B3 situation the wind disturbance as low effect on the motor angular velocity for negative trend data.

7. B5 situation:

   - The lowest rotor angular velocity error is 2.36%decrease is observed at 20% motor speed, and the highest error of 6.28%increase is observed at 40% motor speed. A mean rotor angular velocity error of a 5.8% increase is seen at the B5 situation.
   - The error between the B5 and static measurement is high when compared with B3 which is clearly visible from Table 4.6. It can be concluded that at B5 situation the wind disturbance as high effect on the motor angular velocity for negative trend data.

4.4 Conclusion

1. Till 20% it is observed that the sensor as less error of thrust, drag torque, current and angular velocity. This is because the external disturbances such as motor vibration, external wind effects are not yet into effect. So values are mostly influenced by the measurement noise. However, it can also be seen that when the motor speed increases the effect of external disturbances are more visible. In B1, B2, B3, and B5 there is an external disturbance in effect from the beginning; hence, more information is available, which is in the form of wind along with the measurement noises. However, this also follows the same trend with an increase in speed.

2. Error due to wind disturbance.

   - The highest positive error is observed at the A3 situation; this is because when the propeller is near the ground, the airflow gets congested, a high pressure gets build up beneath the propeller, resulting in high thrust. The mean error at the A3 situation is 9.51% increase when compared with the static test experiment.
   - The highest negative error is seen at the B5 situation; this is because the upper motor pushes the air on the lower one, resulting in building air pressure above the lower propeller. This will create high pressure above the lower propeller; hence, there is a

decrease in thrust. A mean thrust error of a 7.14% decrease is seen at the B5 situation.

- Lowest positive thrust error is at the A1 situation; this is due to very low-pressure increase from the static measurement test beneath the propeller, resulting in a small thrust change compared with other situations. The pressure increase is because of the wall blocking the tip vortex. The mean error at this situation is 3.6% increase when compared with static test experiment.
- Lowest negative thrust error is at B3 situation, here both the rotors face each other vertically. The airflow above the propeller reduces because both the rotors suck the air to generate thrust, resulting in less airflow into the propellers. Thus, less thrust is generated.

3. The thrust, and drag torque measurements as high noise between the motor speed of 60 to 100%; this is because Force/Torque sensor gets influenced by the external noise created by the disturbing object, resulting in high noise.

4. It was observed a maximum deviation of 9.51% increase in thrust when the rotor was placed near the ground. This change is small, for conventional UAVs. However, for the UAVs that are used in interaction tasks require accurate measurement of thrust. To achieve this, a closed-loop thrust controller needs to be designed. To design a closed-loop controller thrust measurement data is needed; this is the motivation to design a thrust estimator. The estimator is designed in chapter 5. An estimator design is based on the rotor angular velocity and current measured by ESC; this will reduce the use of an additional thrust sensor on board of the UAV.

5 Thrust estimator design

In this chapter, a thrust estimator is designed and compared with the experimental data obtained in chapter 4. The estimator is designed based on the systems physical model along with using the rotors acceleration and motor current acquired from embedded sensors. To obtain parameter constants the static data of current, rotor angular velocity, thrust', and drag torque measured in chapter 4 is used. The chapter is divided into six sections, namely; drag torque estimator design, estimated drag torque result comparison, thrust estimator design, estimated design comparison, comparison of measured static method thrust against all other estimated thrust situations, and conclusion. The goals of this section is,

1. *"To design a state variable filter, that will estimate rotor angular acceleration using static rotor angular velocity measured in chapter 4. The estimated rotor acceleration is used to design a thrust estimator."*
2. *"To design an estimator for drag torque by applying Euler's law of motion to rotor disc and motor shaft."*
3. *"To design a thrust estimator from equations 2.1 and 2.3."*
4. *"To analyze the estimated results with experimental results obtained in chapter 4."*

The thrust estimation design as four steps:

Step 1: Acceleration estimator design using state variable filter.
Step 2: Finding motor parameters, using no-load motor condition, and using Euler's law of motion for motor, respectively.
Step 3: Drag torque estimation using the same equation and comparing the results with curve fitted model.
Step 4: Static map design for thrust, using drag torque and thrust relation shown in equation 5.3 and equation5.2.

5.1 Drag torque estimator design

In this section the thrust estimator is designed using physica model of the motor-rotor system. The equation of motor-rotor system is as follows,

$$I\dot{\omega} = \tau - \tau_f - \tau_d \tag{5.1}$$

where,

$$\tau = K_e i \tag{5.2}$$

and drag torque at ideal case is given by,

$$\tau_d = C_T \omega^2 \tag{5.3}$$

from equations 2.1 and 2.3 we can find a relation between thrust and drag torque.

$$T = k\tau_d \tag{5.4}$$

Assuming τ_f equals zero, the shaft torque for a BLDC motor is negligible [49]. From 5.1, the following measurements are required I, $\dot{\omega}$, C_T, ω, i, τ, k_e, τ_d, T, and k. Measurements data of i, ω is provided by ESC. τ_d and T is provided by Force/torque sensor. This data is available from chapter 4. The $\dot{\omega}$ can be derived from ω measurements a state variable filter is designed to estimate it and discussed in subsection 5.1.1. The constant k_e is estimated when no-load is added on the BLDC motor, constant I is estimated analytically using equation 5.1. Both parameter values are compared with estimated data obtained from curve fitting model, the method is shown in subsection 5.1.2.

5.1.1 State variable filter design

A state variable filter is used to estimate the angular acceleration. It helps to estimate the higher derivatives of the output variable. It's operation is performed by using an integral action; this will reduce the noise. A transfer function model is designed using the Matlab system identification toolbox for rotor angular velocity as the output and motor PWM speed as the input. A third-order transfer function was obtained [50]. The obtained transfer function is,

$$G(s) = \frac{622.9}{s^3 + 1.272s^2 + 7.577s + 6.297} \tag{5.5}$$

A fifth-order estimator is designed because higher the order of the filter lesser the noise in the estimated data. The bandwidth of the system in equation 5.5 is 9.72rad/sec. The values of the parameters a0, a1, a2, a3, and a4 where selected such that the bandwidth of the filter is larger than the bandwidth of the signal. The fifth order filter transfer function obtained is,

$$G_f(s) = \frac{a_0}{s^5 + a_4 s^4 + a_3 s^3 + a_2 s^2 + a_1 s + a_0} \tag{5.6}$$

Table 5.1 shows the filter parameters.

Table 5.1: Filter parameters

Parameters	Value
a_0	312500000
a_1	31250000
a_2	1250000
a_3	25000
a_4	250

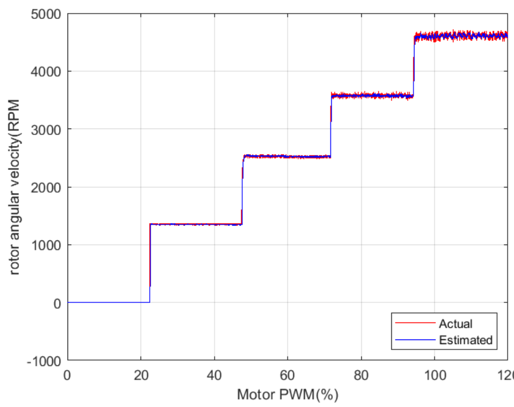

(a) Filtered angular velocity vs actual angular velocity.

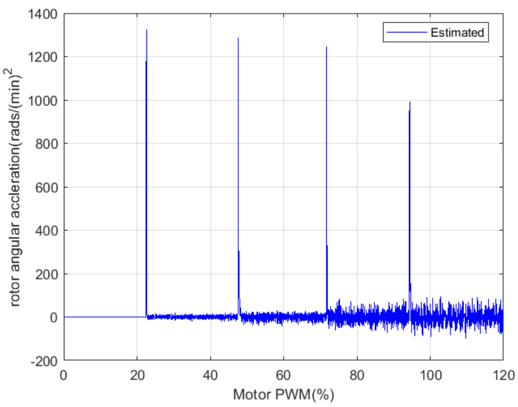

(b) Estimated angular acceleration using state variable filter

Figure 5.1: Estimated angular velocity and estimated angular acceleration using state variable filter.

5.1.2 Drag torque estimation design

In this subsection, a drag torque estimator is designed from the relation shown in equation 5.1. To find the unknown parameter k_e no-load condition of the motor is used, a schematic and the experimental setup of no-load method is shown in the Figure 5.2. At no-load condition τ_d is zero. Equation 5.1 can be simplified as

$$\tau = I\hat{\dot{\omega}} \tag{5.7}$$

τ data is measured from Force/torque sensor, and from subsection 5.1.1 the state variable filter design will estimate rotor angular acceleration from rotor angular velocity obtained from no-load condition. By the analytical method, the rotor moment of inertia can be obtained as a mean value of 1.8473×10^{-4} and a standard deviation of 1.6065×10^{-6}.

Figure 5.2: Experimental setup of no-load system.

The parameter k_t is obtained from the static test measurement data of drag torque obtained from chapter 4 and an estimated rotor angular acceleration for the static test. The known variables from equation 5.1 are $\hat{\dot{\omega}}$, τ_d and parameter I, so analytically k_t can be derived and it is 18.9270×10^{-3} mean and a standard deviation of 4.657×10^{-3} is obtained.

To reduce the error between the static method and estimated method, a second-order polynomial is used. This decreases the error to get an approximate match. As the curve fitted model showed less error, therefore the estimator is designed based on the curve fitted model. The block diagram shown in the Figure 5.5 gives an overview of the drag torque estimator design. Table 4.1 shows the model that is selected to design the estimator. From the Figure 4.16b and 4.17b a low sensor noise is observed, therefore current filter is not designed, ESC current sensor data and estimated rotor angular acceleration is used to design the estimator.

The Figure 5.3 shows a 3d plot comparing the static experiment method result with the curve fitted model and analytical method. The error in analytical method is due to the down-sampling of the initially collected data-set. This filtering retained the measurements that contributed to the system model that represents a static condition. The error in the curve fitted model is due to the curve fitting error for the static condition because of high noise in the drag torque measurement, analyzed in chapter 4.

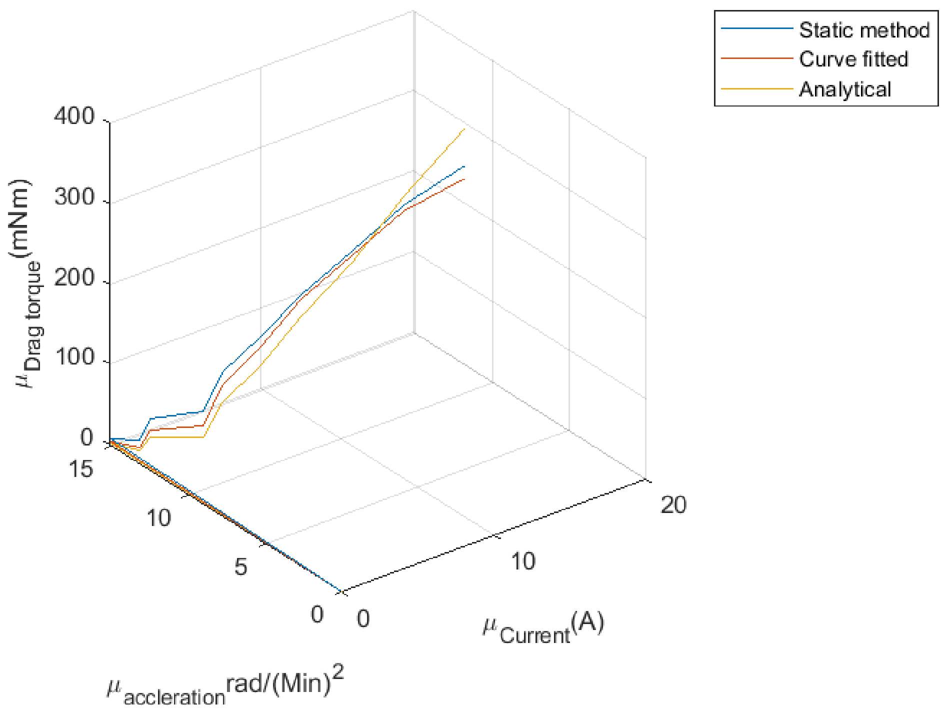

Figure 5.3: 3d plot showing comparison between static, curve fitted model and analytical model.

Table 5.2 shows the parameters derived from the curve fitted and analytical method.

Table 5.2: Motor-rotor aerodynamic parameters

Parameters	Analytical($\hat{\tau}_d = k_e i - I\hat{\omega}$)	Curve Fitting($\hat{\tau}_d = k_e i + k_{e1} i^2 + k_{ei} i\hat{\omega} + I\hat{\omega}$)
$I(kgm^2)$	1.8473×10^{-4}	0.1545×10^{-3}
$k_e(Nm/A)$	18.9270×10^{-3}	25.76×10^{-3}
k_{e1}	0	-0.6965×10^{-3}
k_{ei}	0	0.2824×10^{-3}

- The lowest drag torque error of 4.43 %decrease is observed at 90% motor speed, and the highest error of 63.3%increase is observed at 10% motor speed. A mean drag torque error of 9.02% decrease is seen at the analytical estimated model.

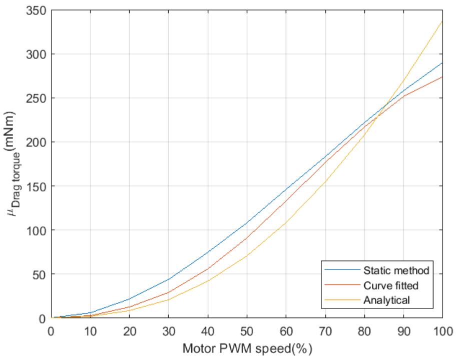

Figure 5.4: Measured, curve fitted estimated, and estimated analytical drag torque at static position test for PWM motor speed ranging between 0% to 100%.

PWM	$\mu_{\tau_d} \times 10^{-3}$	$\mu_{\hat{\tau}_d} \times 10^{-3}$	$E_{\mu_{\tau_d}-\mu_{\hat{\tau}_d}} \times 10^{-3}$
0	0	0	0
10	6.1146	2.2604	3.8541
20	21.8343	8.8391	13.0436
30	44.2706	20.9176	23.0761
40	74.5448	41.7679	32.7768
50	108.6436	70.3636	38.2799
60	145.663	108.5098	37.1531
70	184.2408	154.9043	28.4304
80	221.5354	208.2590	14.0729
90	258.1973	269.7524	-11.5551
100	290.0902	337.0468	-47.0574

Table 5.3: Comparison table of measured, estimated curve fitted, and analytical estimated mean drag torque at static position for motor PWM ranging between 0 and 100%. The color code in the table shows lowest error value and highest error value drag torque error values.

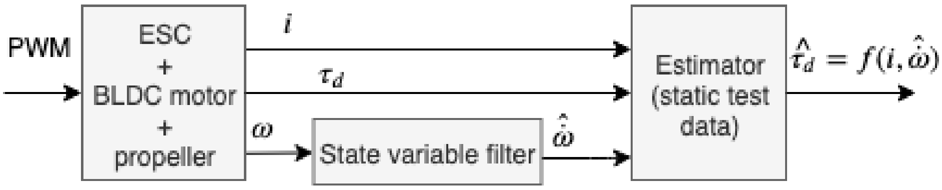

Figure 5.5: Block diagram showing torque estimator design, the estimator is designed using curve fitting.

5.2 Results and comparison of estimated drag torque

In this section, the comparison between the measurement and estimated drag torque is discussed. From Figure 5.6 to Figure 5.13 shows the comparison of measurement and experimental drag torque at different situations for motor speed ranging between 0 to 100%. From Table 5.4 to Table 5.11 shows the comparison table of experimental and estimated drag torque at different experimental situations. The color code in these tables lowest error value and highest error value drag torque error values. The summary of different experimental situation is in Table 4.1.

5.2.1 Static situation

1. The Figure 5.6 shows the mean of the measured and estimated plot of drag torque at static situation. The mean of drag torque is plotted for better understanding. Table 5.4 shows the mean of measured drag torque, estimated drag torque, and estimated error for motor speed between 0 to 100%.
2. The lowest drag torque error of 1.802% increase is observed at 80% motor speed, and the highest error of 47.22% increase is observed at 10% motor speed. A mean drag torque error of a 7.51% increase is seen at the curve fitted estimated model.
3. The error is because of curve fitting error at static condition.

4. The estimated model as high error for motor speed between 10% to 60% and the lowest error between 70% to 90% of motor speed. This is because of the curve fitting.

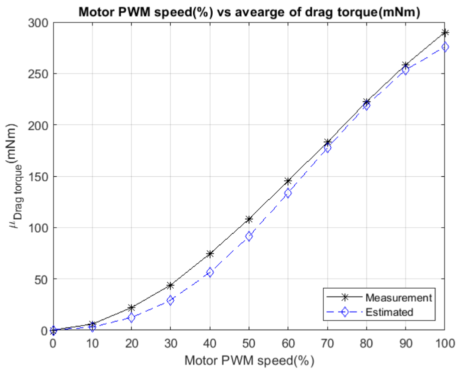

Figure 5.6: Comparison plot of measurement and estimated mean drag torque at static position.

PWM	$\mu_{\tau_d} \times 10^{-3}$	$\mu_{\hat{\tau}_d} \times 10^{-3}$	$E_{\mu_{\tau_d}-\mu_{\hat{\tau}_d}} \times 10^{-3}$
0	0	0	0
10	6.1146	3.2271	2.8875
20	21.8343	21.5030	9.3798
30	44.2706	29.1247	14.8691
40	74.5322	56.5689	17.9759
50	108.1980	91.6386	17.0050
60	145.9054	133.7923	11.8697
70	184.2408	177.9323	5.4025
80	221.5342	219.0196	3.3124
90	258.5097	253.5369	4.6604
100	290.0902	275.5562	14.4332

Table 5.4: Comparison table of measurement and estimated mean drag torque at static position.

5.2.2 A1 situation

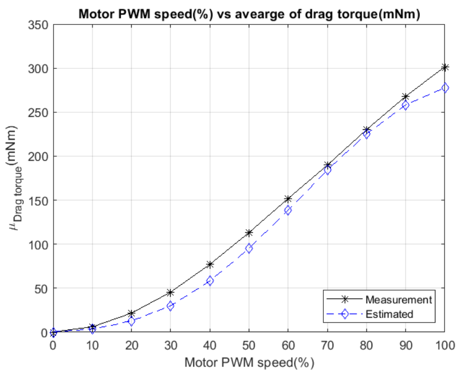

Figure 5.7: Comparison plot of measurement and estimated mean drag torque at A1 position.

PWM	$\mu_{\tau_d} \times 10^{-3}$	$\mu_{\hat{\tau}_d} \times 10^{-3}$	$E_{\mu_{\tau_d}-\mu_{\hat{\tau}_d}} \times 10^{-3}$
0	0	0	0
10	6.3408	3.3642	2.9765
20	21.8679	12.3125	9.5553
30	45.4315	29.9169	15.5154
40	77.1719	58.7693	18.4025
50	112.9177	94.8864	18.0312
60	151.4921	138.8500	12.6420
70	190.2710	184.2137	6.0572
80	230.2773	225.6946	4.5826
90	267.4687	258.2378	9.2308
100	300.9717	277.7677	23.2039

Table 5.5: Comparison table of measurement and estimated mean drag torque at A1 position.

1. The Figure 5.7 shows the mean of the measured and estimated plot of drag torque at A1 situation. The mean of drag torque is plotted for better understanding. Table 5.5 shows the mean of measured drag torque, estimated drag torque, and estimated error for motor speed between 0 to 100%.

2. The lowest drag torque error of a 1.98% increase is observed at 80% motor speed, and the highest error of a 46.94% increase is observed at 10% motor speed. A mean drag torque error of a 8.56% increase is seen at the A1 estimated model.

3. The error is because of curve fitting error and losses occur during physical domain transmission.

5.2.3 A2 situation

1. The Figure 5.8 shows the mean of the measured and estimated plot of drag torque at the A2 situation. The mean of drag torque is plotted for better understanding. Table 5.6

shows the mean of measured drag torque, estimated drag torque, and estimated error for motor speed between 0 to 100%.

2. The lowest drag torque error of a 1.91% increase is observed at the 80% motor speed, and the highest error of a 44.04% increase is observed at 10% motor speed. A mean drag torque error of 8.66% increase is seen at the A2 estimated model.

3. The error is because of curve fitting error and losses occur during physical domain transmission.

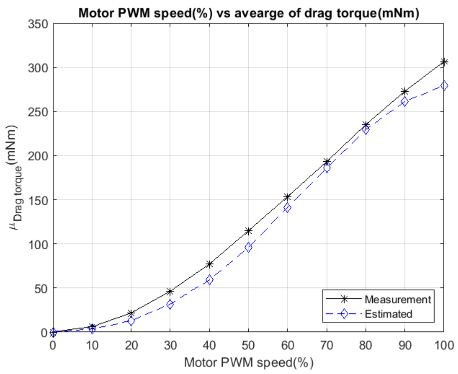

Figure 5.8: Comparison plot of measurement and estimated mean drag torque at A2 position.

PWM	$\mu_{\tau_d} \times 10^{-3}$	$\mu_{\hat{\tau}_d} \times 10^{-3}$	$E_{\mu_{\tau_d}-\mu_{\hat{\tau}_d}} \times 10^{-3}$
0	0	0	0
10	6.2089	3.4745	2.7343
20	21.8763	12.3469	9.5293
30	46.2398	31.3003	14.9394
40	77.0938	60.6594	16.4343
50	114.8362	94.5227	20.3134
60	153.4657	141.2890	12.1766
70	193.2848	187.7034	5.5813
80	234.9879	230.4994	4.4884
90	273.0334	260.7216	12.3118
100	306.5187	278.9804	27.5383

Table 5.6: Comparison table of measurement and estimated mean drag torque at A2 position.

5.2.4 A3 situation

1. The Figure 5.9 shows the mean of the measured and estimated plot of drag torque at the A3 situation. The mean of drag torque is plotted for better understanding. Table 5.7 shows the mean of measured drag torque, estimated drag torque, and estimated error for motor speed between 0 to 100%.

2. The lowest drag torque error of a 5.65% increase is observed at 70% motor speed, and the highest error of a 50.29% increase is observed at 10% motor speed. A mean drag torque error of a 11.66% increase is seen at the A3 estimated model.

3. The error is because of curve fitting error and losses occur during physical domain transmission.

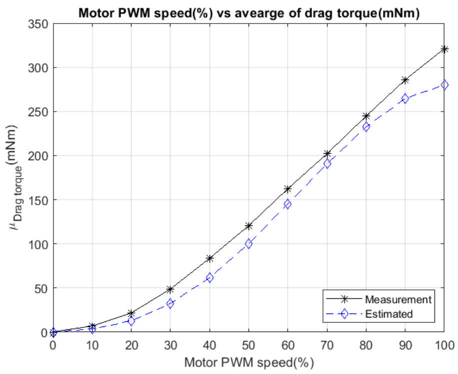

Figure 5.9: Comparison plot of measurement and estimated mean drag torque at A3 position.

PWM	$\mu_{\tau_d} \times 10^{-3}$	$\mu_{\hat{\tau}_d} \times 10^{-3}$	μ_{τ_d} - $\mu_{\hat{\tau}_d} \times 10^{-3}$
0	0	0	0
10	6.7205	3.3400	3.3804
20	21.8276	12.4845	9.3430
30	48.391	31.9496	16.4413
40	83.4969	61.6840	21.8128
50	120.2175	99.8121	20.4053
60	162.6000	144.8176	17.7823
70	202.5278	191.0802	11.4475
80	244.8540	232.2486	12.6053
90	286.0024	264.7367	21.2656
100	320.6702	280.3965	40.2736

Table 5.7: Comparison table of measurement and estimated mean drag torque at A3 position.

5.2.5 B1 situation

1. The Figure 5.10 shows the mean of the measured and estimated plot of drag torque at the B1 situation. The mean of drag torque is plotted for better understanding. Table 5.8 shows mean of measured drag torque, estimated drag torque, and estimated error for motor speed between 0 to 100%.

2. The lowest drag torque error of a 3.524% increase is observed at 70% motor speed, and the highest error of a 45.81% increase is observed at 10% motor speed. A mean drag torque error of a 9.43% increase is seen at the B1 estimated model.

3. The error is because of curve fitting error and losses occur during physical domain transmission.

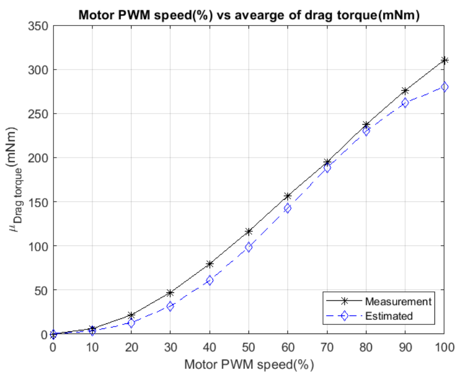

Figure 5.10: Comparison plot of measurement and estimated mean drag torque at B1 position.

PWM	$\mu_{\tau_d} \times 10^{-3}$	$\mu_{\hat{\tau}_d} \times 10^{-3}$	$E_{\mu_{\tau_d}-\mu_{\hat{\tau}_d}} \times 10^{-3}$
0	0	0	0
10	6.4365	3.4876	2.9488
20	21.8044	12.4818	9.3225
30	46.9790	31.4125	15.5664
40	79.6100	60.8727	18.7372
50	116.1400	98.2721	17.8678
60	156.5693	142.7552	13.814
70	195.4113	188.5243	6.8870
80	237.2059	229.8556	7.3502
90	276.2573	262.4909	13.7663
100	309.9986	279.7946	30.2039

Table 5.8: Comparison table of measurement and estimated mean drag torque at B1 position.

5.2.6 B2 situation

1. The Figure 5.11 shows the mean of the measured and estimated plot of drag torque at the B2 situation. The mean of drag torque is plotted for better understanding. Table 5.9 shows mean of measured drag torque, estimated drag torque, and estimated error for motor speed between 0 to 100%.

2. The lowest drag torque error of a 3.516% increase is observed at 80% motor speed, and the highest error of a 52.92% increase is observed at 20% motor speed. A mean drag torque error of a 9.38% increase is seen at the B2 estimated model.

3. The error is because of curve fitting error and losses occur during physical domain transmission.

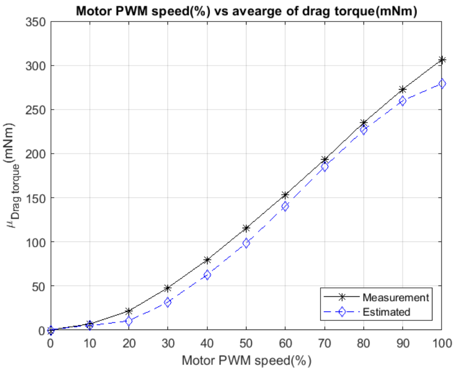

Figure 5.11: Comparison plot of measurement and estimated mean drag torque at B2 position.

PWM	$\mu_{\tau_d} \times 10^{-3}$	$\mu_{\hat{\tau}_d} \times 10^{-3}$	$E_{\mu_{\tau_d}-\mu_{\hat{\tau}_d}} \times 10^{-3}$
0	0	0	0
10	6.6570	5.0803	1.5766
20	21.6574	10.1941	11.4632
30	47.7830	31.4125	16.3704
40	80.1079	62.3267	17.7811
50	116.0286	98.8065	17.2220
60	153.5570	140.2389	13.3180
70	193.2102	185.1005	8.1096
80	234.7825	226.5266	8.2558
90	272.5951	259.6768	12.9182
100	306.2288	278.8665	27.3622

Table 5.9: Comparison table of measurement and estimated mean drag torque at B2 position.

5.2.7 B3 situation

1. The Figure 5.12 shows the mean of the measured and estimated plot of drag torque at the B3 situation. The mean of drag torque is plotted for better understanding. Table 5.10 shows the mean of measured drag torque, estimated drag torque, and estimated error for motor speed between 0 to 100%.

2. The lowest drag torque error of a 0.0622% increase is observed at 80% motor speed, and the highest error of a 47.7% increase is observed at 10% motor speed. A mean drag torque error of a 6.07% increase is seen at the B3 estimated model.

3. The error is because of curve fitting error and losses occur during physical domain transmission.

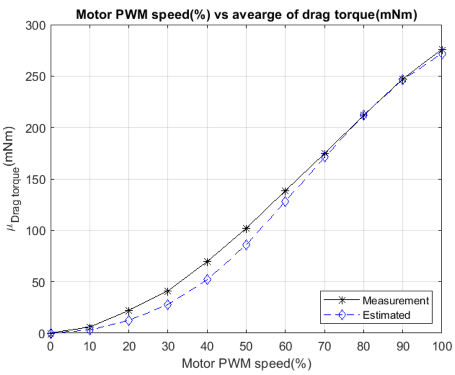

Figure 5.12: Comparison plot of measurement and estimated mean drag torque at B3 position.

PWM	$\mu_{\tau_d} \times 10^{-3}$	$\mu_{\hat{\tau}_d} \times 10^{-3}$	$E_{\mu_{\tau_d}-\mu_{\hat{\tau}_d}} \times 10^{-3}$
0	0	0	0
10	5.7089	2.9854	2.7234
20	21.9769	12.5903	9.3865
30	40.7942	27.5257	13.2684
40	69.6176	52.1868	17.4307
50	102.2115	85.9098	16.3016
60	138.6799	127.9218	10.75802
70	175.1681	171.1087	4.05930
80	212.2154	212.0832	0.1321
90	246.9875	246.6316	0.3558
100	275.6900	271.8110	3.8789

Table 5.10: Comparison table of measurement and estimated mean drag torque at B3 position.

5.2.8 B5 situation

1. The Figure 5.13 shows the mean of the measured and estimated plot of drag torque at B5 situation. The mean of drag torque is plotted for better understanding. Table 5.11 shows the mean of measured drag torque, estimated drag torque, and estimated error for motor speed between 0 to 100%.
2. The lowest drag torque error of a 0.0083% decrease is observed at 100% motor speed, and the highest error of a 45.16% increase is observed at 10% motor speed. A mean drag torque error of a 1.63% increase is seen at the B5 estimated model.
3. The error is because of curve fitting error and losses occur during physical domain transmission.

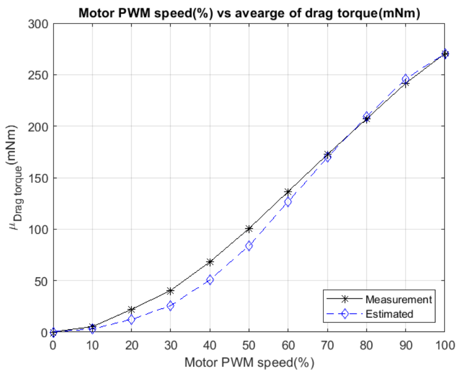

Figure 5.13: Comparison plot of measurement and estimated mean drag torque at B5 position.

PWM	$\mu_{\tau_d} \times 10^{-3}$	$\mu_{\hat{\tau}_d} \times 10^{-3}$	$E_{\mu_{\tau_d}-\mu_{\hat{\tau}_d}} \times 10^{-3}$
0	0	0	0
10	5.4927	3.0117	2.4809
20	21.9921	12.5374	9.4546
30	39.9583	25.8603	14.0979
40	68.3013	96.9492	17.7683
50	100.2472	83.8022	16.4449
60	136.3947	126.1684	10.2262
70	173.0847	169.9335	3.1511
80	206.9911	209.5486	-2.5575
90	241.3817	245.4016	-4.0199
100	269.9802	270.0028	-0.0226

Table 5.11: Comparison table of measurement and estimated mean drag torque at B5 position.

5.2.9 Drag torque error bar analysis

1. A negligible error difference between the estimated static and other estimated situations is seen when motor speed is between 10 to 50%.
2. At motor speed between 60% to 100% there is a deviation in error bars; this is because of high motor vibrations due to disturbing object, that effect the thrust and drag torque measurement data obtained in chapter 4. Hence a increasing trend is seen.

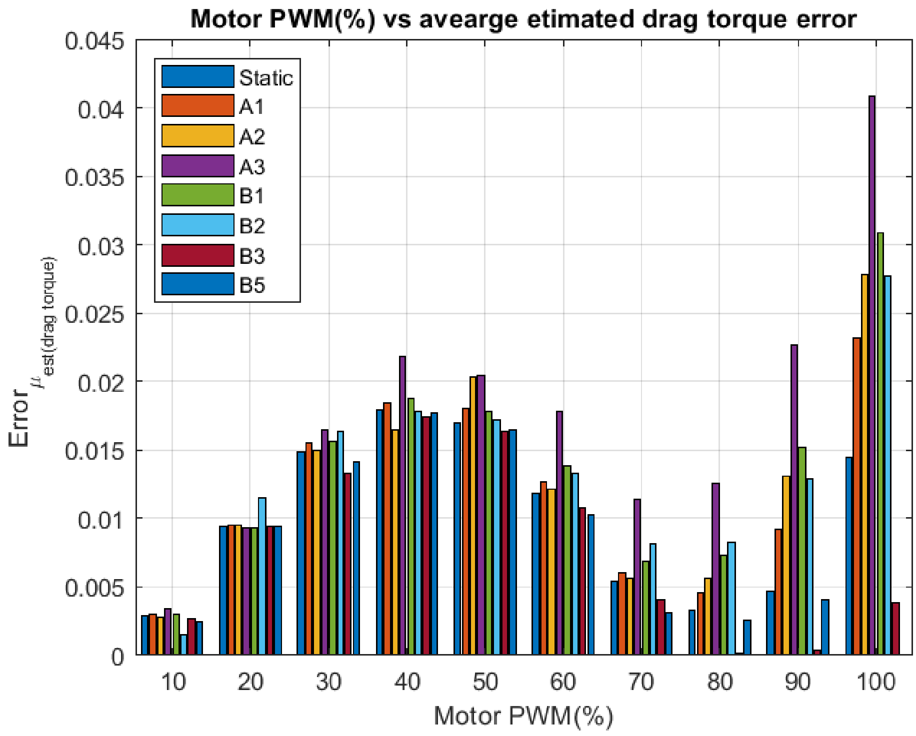

Figure 5.14: Error bar plot showing drag torque estimation error.

5.3 Thrust estimation design

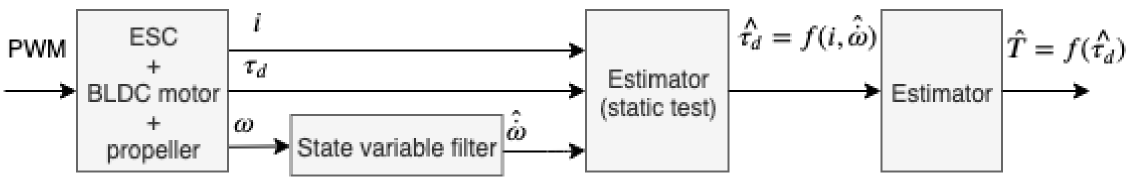

Figure 5.15: Block diagram showing thrust estimator design. The estimator is designed using Matlab curve fitting toolbox.

The thrust estimator is designed from the estimated drag torque designed in section 5.1.2. The ideal rotor relation is used to design the thrust estimator. The Figure 5.15 shows the block diagram of the estimator. A curve fitting toolbox from Matlab is used to design the estimator.The Figure 5.16 shows a linear relationship between mean drag torque and mean thrust. For better results, the quadratic equation is used to estimate the thrust. In chapter 4.4 it was observed that the thrust and drag torque are directly proportional. So, any change that is caused by external drag on the motor-rotor system will change the drag torque, resulting in change in thrust.

Table 5.12: Motor-rotor aerodynamic parameters

Parameters	Curve Fitting($\hat{T} = k_1\hat{\tau}_d^2 + k_2\hat{\tau}_d$)
k_1	-0.07874
k_2	4.778

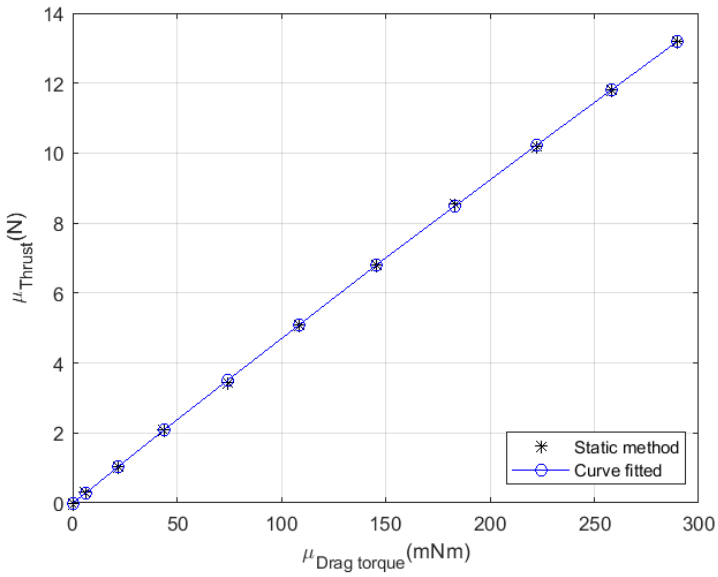

Figure 5.16: Drag torque vs estimated thrust plot. The plot is a comparison of estimated thrust with measured thrust static model.

5.4 Results and comparison of estimated thrust

In this section, the comparison between the measurement and estimated thrust is discussed. From Figure 5.17 to Figure 5.24 shows the comparison of measurement and experimental thrust at different situations for motor speed ranging between 0 to 100%. From Table 5.4 to Table 5.11 shows the comparison table of experimental and estimated thrust at different experimental situations. The color code in these tables lowest error value and highest error value thrust error values. The summary of different experimental situation is in Table 4.1.

5.4.1 Static situation

1. The Figure 5.17 shows the mean of the measured and estimated plot of thrust at the static situation. The mean of thrust is plotted for better understanding. Table 5.13 shows the mean of measured thrust, estimated thrust, and estimated error for motor speed between 0 to 100%.

2. The lowest thrust error of a 0.9466% increase is observed at 80% motor speed, and the highest error of a 49.90% increase is observed at 10% motor speed. A mean thrust error of a 7.44% increase is seen at the static estimated model.

3. The error is because of curve fitting error while designing the drag torque estimator, and thrust estimator.

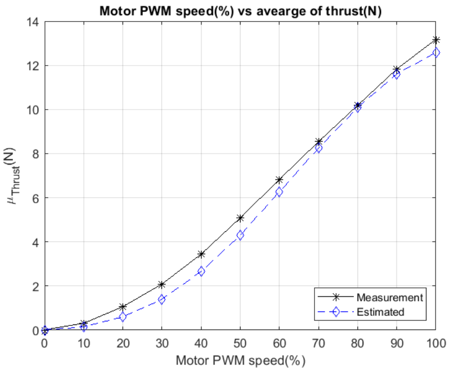

Figure 5.17: Comparison plot of measurement and estimated mean thrust at static position.

PWM	μ_T	$\mu_{\hat{T}}$	$E_{\mu_T - \mu_{\hat{T}}}$
0	0	0	0
10	0.3078	0.1541	0.1536
20	1.0513	0.5961	0.4551
30	2.0832	1.3848	0.6983
40	3.4586	2.6776	0.7809
50	5.0739	4.3123	0.7615
60	6.8159	6.2516	0.5642
70	8.5644	8.2523	0.3120
80	10.1833	10.0870	0.0962
90	11.8239	11.6078	0.2160
100	13.1821	12.5681	0.6139

Table 5.13: Comparison table of measurement and estimated mean thrust at static position.

5.4.2 A1 situation

1. The Figure 5.18 shows the mean of the measured and estimated plot of thrust at the A1 situation. The mean of thrust is plotted for better understanding. Table 5.14 shows the mean of measured thrust, estimated thrust, and estimated error for motor speed between 0 to 100%.

2. The lowest thrust error of a 1.869% increase is observed at 80% motor speed, and the highest error of a 49.74% increase is observed at 10% motor speed. A mean thrust error of a 8.58% increase is seen at the A1 estimated model.

3. The error is because of curve fitting error while designing the drag torque estimator, and thrust estimator. The other reason is because of losses occur during physical domain transmission.

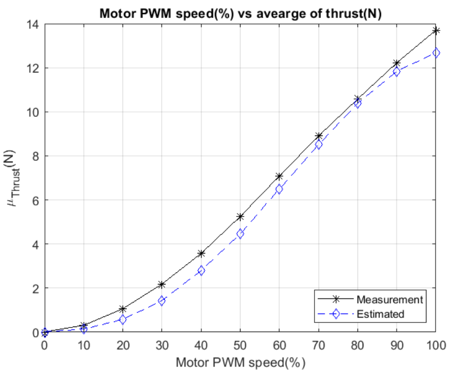

Figure 5.18: Comparison plot of measurement and estimated mean thrust at A1 position.

PWM	μ_T	$\mu_{\hat{T}}$	$E_{\mu_T - \mu_{\hat{T}}}$
0	0	0	0
10	0.3198	0.1606	0.1591
20	1.0502	0.5871	0.4631
30	2.1634	1.4223	0.7411
40	3.5934	2.7808	0.8126
50	5.2617	4.4627	0.7990
60	7.0759	6.4824	0.5934
70	8.8984	8.5345	0.3638
80	10.5804	10.3826	0.1978
90	12.2150	11.8135	0.4014
100	13.6962	12.6642	1.0319

Table 5.14: Comparison table of measurement and estimated mean thrust at A1 position.

5.4.3 A2 situation

1. The Figure 5.19 shows the mean of the measured and estimated plot of thrust at the A2 situation. The mean of thrust is plotted for better understanding. Table 5.15 shows the mean of measured thrust, estimated thrust, and estimated error for motor speed between 0 to 100%.

2. The lowest thrust error of a 0.2657% increase is observed at 80% motor speed, and the highest error of a 49.02% increase is observed at 10% motor speed. A mean thrust error of a 9.28% increase is seen at the A2 estimated model.

3. The error is because of curve fitting error while designing the drag torque estimator, and thrust estimator. The other reason is because of losses occur during physical domain transmission.

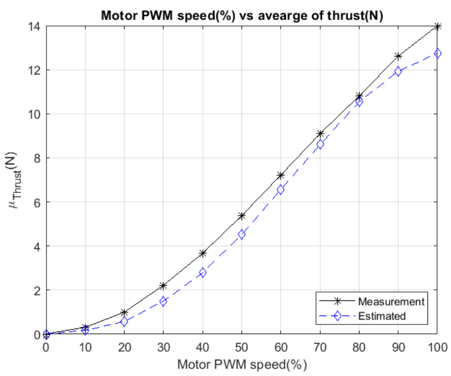

Figure 5.19: Comparison plot of measurement and estimated mean thrust at A2 position.

PWM	μ_T	$\mu_{\hat{T}}$	$E_{\mu_T - \mu_{\hat{T}}}$
0	0	0	0
10	0.3266	0.1659	0.1607
20	1.0068	0.5887	0.4180
30	2.2209	1.4878	0.7330
40	3.6706	2.8693	0.8012
50	5.3849	4.4459	0.9389
60	7.2137	6.5936	0.6200
70	9.1093	8.6910	0.4182
80	10.8075	10.5949	0.2126
90	12.6080	12.0002	0.6077
100	13.9901	12.7464	1.2436

Table 5.15: Comparison table of measurement and estimated mean thrust at A2 position.

5.4.4 A3 situation

1. The Figure 5.20 shows the mean of the measured and estimated plot of thrust at the A3 situation. The mean of thrust is plotted for better understanding. Table 5.16 shows mean of measured thrust, estimated thrust, and estimated error for motor speed between 0 to 100%.

2. The lowest thrust error of a 5.234% increase is observed at 80% motor speed, and the highest error of a 48.59% increase is observed at 10% motor speed. A mean thrust error of a 9.28% increase is seen at the A3 estimated model.

3. The error is because of curve fitting error while designing the drag torque estimator, and thrust estimator. The other reason is because of losses occur during physical domain transmission.

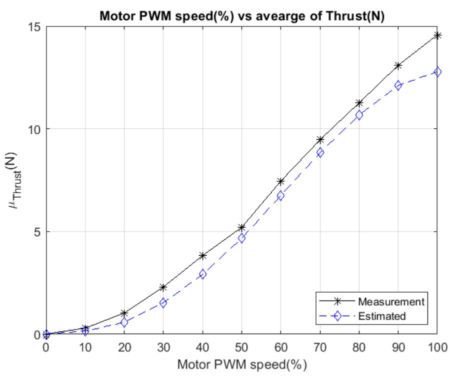

Figure 5.20: Comparison plot of measurement and estimated mean thrust at A3 position.

PWM	μ_T	$\mu_{\hat{T}}$	$E_{\mu_T - \mu_{\hat{T}}}$
0	0	0	0
10	0.3103	0.1594	0.1508
20	1.0399	0.5952	0.4446
30	2.2838	1.5185	0.7652
40	3.8246	2.9173	0.9073
50	5.2112	4.6905	0.5206
60	7.4377	6.7542	0.6834
70	9.4703	8.8423	0.6280
80	11.2617	10.6721	0.5895
90	13.0760	12.0972	0.9787
100	14.5780	12.7782	1.7998

Table 5.16: Comparison table of measurement and estimated mean thrust at A3 position.

5.4.5 B1 situation

1. The Figure 5.21 shows the mean of the measured and estimated plot of thrust at the B1 situation. The mean of thrust is plotted for better understanding. Table 5.17 shows mean of measured thrust, estimated thrust, and estimated error for motor speed between 0 to 100%.

2. The lowest thrust error of a 3.43% increase is observed at 80% motor speed, and the highest error of a 49.54% increase is observed at 10% motor speed. A mean thrust error of a 10.17% increase is seen at the B1 estimated model.

3. The error is because of curve fitting error while designing the drag torque estimator, and thrust estimator. The other reason is because of losses occur during physical domain transmission.

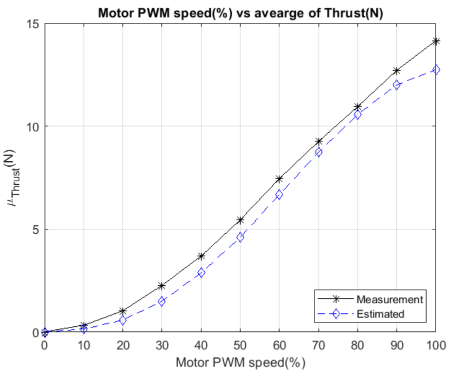

Figure 5.21: Comparison plot of measurement and estimated mean thrust at B1 position.

PWM	μ_T	$\mu_{\hat{T}}$	$E_{\mu_T - \mu_{\hat{T}}}$
0	0	0	0
10	0.3302	0.1665	0.1636
20	1.0496	0.5951	0.4544
30	2.2448	1.4931	0.7516
40	3.7103	2.8793	0.8309
50	5.4642	4.6194	0.8447
60	7.4520	6.6603	0.7916
70	9.2528	8.7278	0.5249
80	10.9446	10.5664	0.3781
90	12.7146	11.999	0.7153
100	14.1417	12.7521	1.385

Table 5.17: Comparison table of measurement and estimated mean thrust at B1 position.

5.4.6 B2 situation

1. The Figure 5.22 shows the mean of the measured and estimated plot of thrust at the B2 situation. The mean of thrust is plotted for better understanding. Table 5.18 shows the mean of measured thrust, estimated thrust, and estimated error for motor speed between 0 to 100%.

2. The lowest thrust error of a 3.05% increase is observed at 80% motor speed, and the highest error of a 50.98% increase is observed at 20% motor speed. A mean thrust error of a 9.52% increase is seen at the B2 estimated model.

3. The error is because of curve fitting error while designing the drag torque estimator, and thrust estimator. The other reason is because of losses occur during physical domain transmission.

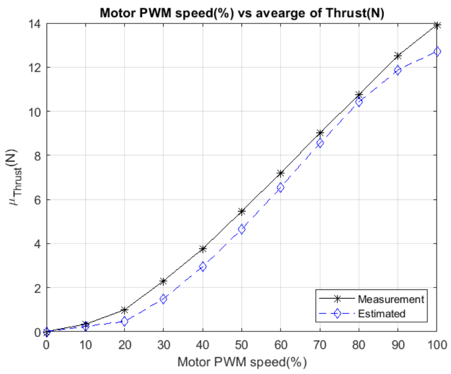

Figure 5.22: Comparison plot of measurement and estimated mean thrust at B2 position.

PWM	μ_T	$\mu_{\hat{T}}$	$E_{\mu_T - \mu_{\hat{T}}}$
0	0	0	0
10	0.3351	0.2425	0.0926
20	0.9921	0.4862	0.5058
30	2.2906	1.493	0.7974
40	3.7536	2.9473	0.8062
50	5.4540	4.6441	0.8098
60	7.2102	6.5457	0.6644
70	9.0273	8.5743	0.4529
80	10.7475	10.4193	0.3281
90	12.5106	11.8763	0.6342
100	13.9254	12.7119	1.2134

Table 5.18: Comparison table of measurement and estimated mean thrust at B2 position.

5.4.7 B3 situation

1. The Figure 5.23 shows the mean of the measured and estimated plot of thrust at the B3 situation. The mean of thrust is plotted for better understanding. Table 5.19 shows the mean of measured thrust, estimated thrust, and estimated error for motor speed between 0 to 100%.

2. The lowest thrust error of a 0.025% decrease is observed at 90% motor speed, and the highest error of a 51.11% increase is observed at 10% motor speed. A mean thrust error of a 5.69% increase is seen at the B3 estimated model.

3. The error is because of curve fitting error while designing the drag torque estimator, and thrust estimator. The other reason is because of losses occur during physical domain transmission.

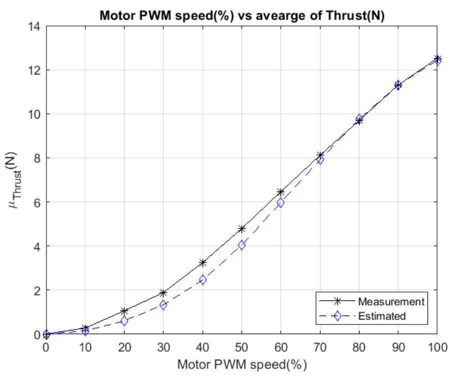

Figure 5.23: Comparison plot of measurement and estimated mean thrust at B3 position.

PWM	μ_T	$\mu_{\hat{T}}$	$E_{\mu_T - \mu_{\hat{T}}}$
0	0	0	0
10	0.2919	0.1425	0.1494
20	1.0533	0.6003	0.4529
30	1.8962	1.3092	0.5869
40	3.2409	2.4720	0.7688
50	4.7860	4.0466	0.7393
60	6.4656	5.9832	0.4823
70	8.1441	7.9450	0.1991
80	9.6832	9.7791	-0.0959
90	11.3022	11.3051	-0.0029
100	12.5046	12.4053	0.0992

Table 5.19: Comparison table of measurement and estimated mean thrust at B3 position.

5.4.8 B5 situation

1. The Figure 5.24 shows the mean of the measured and estimated plot of thrust at the B5 situation. The mean of thrust is plotted for better understanding. Table 5.20 shows the mean of measured thrust, estimated thrust, and estimated error for motor speed between 0 to 100%.

2. The lowest thrust error of a 0.44% decrease is observed at 100% motor speed, and the highest error of a 51.181% increase is observed at 10% motor speed. An mean thrust error of a 0.97% increase is seen at the B5 estimated model.

3. The error is because of curve fitting error while designing the drag torque estimator, and thrust estimator. The other reason is because of losses occur during physical domain transmission.

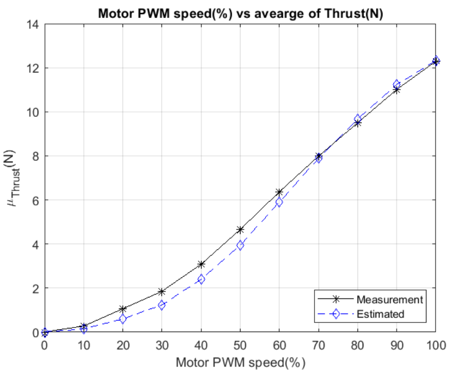

Figure 5.24: Comparison plot of measurement and estimated mean thrust at B5 position.

PWM	μ_T	$\mu_{\hat{T}}$	$E_{\mu_T-\mu_{\hat{T}}}$
0	0	0	0
10	0.2766	0.1438	0.1327
20	1.0621	0.5978	0.4642
30	1.8395	1.2303	0.6091
40	3.1000	4.5582	0.7056
50	4.6630	3.9487	0.7142
60	6.3757	5.9029	0.4727
70	7.9935	7.8920	0.1014
80	9.4907	9.6664	-0.1757
90	11.0081	11.2511	-0.2430
100	12.2726	12.3267	-0.0541

Table 5.20: Comparison table of measurement and estimated mean thrust at B5 position.

5.4.9 Analysis of error bar plot

The Figure 5.25 shows the absolute error bar plot of estimated values.

1. A negligible error difference between the estimated static and other estimated situations is seen when motor speed is between 10 to 50%.

2. At motor speed between 60% to 100% there is a deviation in error bars; this is because of high motor vibrations due to disturbing object, that effect the thrust and drag torque measurement data obtained in chapter 4. Hence a increasing trend is seen.

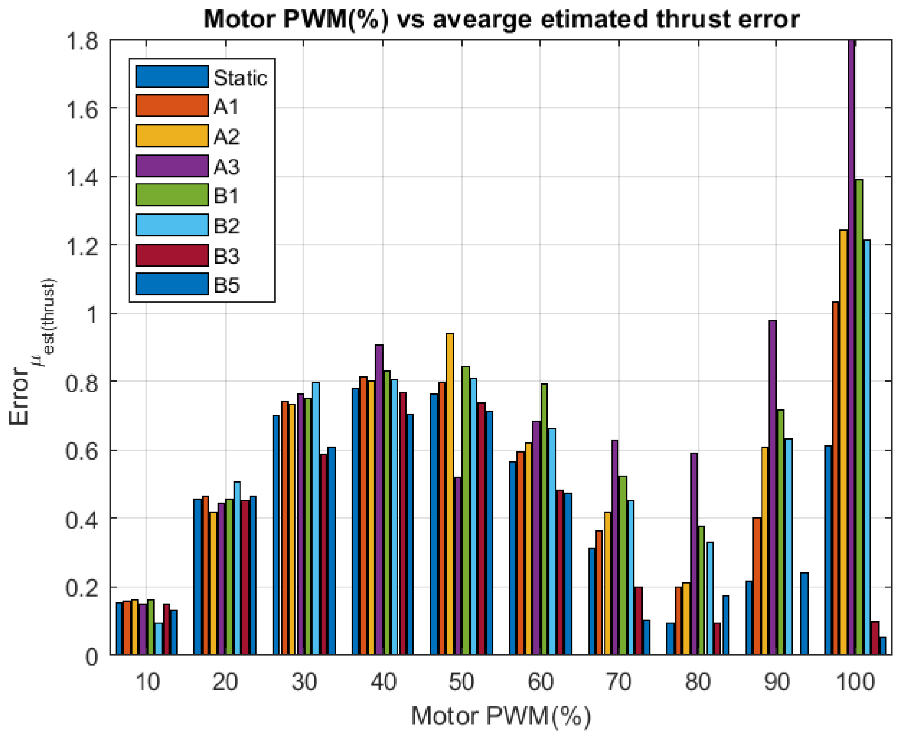

Figure 5.25: Error bar plot showing thrust estimation error.

5.5 Comparison of measured static method against all estimated situations

In this section a the static measurement thrust data obtained in chapter 4 is compared with estimated thrust data. Table 5.21 shows the comparison between the estimated thrust measurements with the measurement static thrust data obtained in chapter 4 and the Figure 5.26 shows the error bar plot of the compared data. The comparison is made with the Table 4.2.

Table 5.21: Comparison of mean static condition thrust data with estimated different experimental test condition mean thrust data for motor PWM ranging between 0 to 100 %. The table shows the error between estimated situation and static measurement obtained in 4.3.1, i.e . $E_{(A1)} = \hat{T}_{A1} - T_{Static}$.

PWM	$E_{(A1)}$	$E_{(A2)}$	$E_{(A3)}$	$E_{(B1)}$	$E_{(B2)}$	$E_{(B3)}$	$E_{(B5)}$
0	0	0	0	0	0	0	0
10	-0.1471	-0.1418	-0.1483	-0.1412	-0.0652	-0.1652	-0.1639
20	-0.4641	-0.4625	-0.4560	-0.4561	-0.56504	-0.4509	-0.4534
30	-0.6608	-0.5953	-0.5646	-0.5900	-0.5900	-0.7739	-0.8528
40	-0.6777	-0.6668	-0.5412	-0.5792	-0.5112	-0.9865	1.0996
50	-0.6111	-0.5566	-0.3833	-0.4544	-0.4297	-1.0272	-1.1251
60	- 0.3334	-0.2484	-0.0616	-0.1555	-0.2701	-0.8326	-0.9129
70	- 0.0298	0.0563	0.2779	0.1634	0.0099	-0.6193	-0.6723
80	0.1993	0.3605	0.4888	0.3831	0.2360	-0.4041	-0.5168
90	- 0.0103	0.1140	0.2733	0.1753	0.0524	-0.5187	-0.5727
100	-0.5178	-0.4548	-0.4184	-0.4388	-0.4701	-0.7760	-0.8343

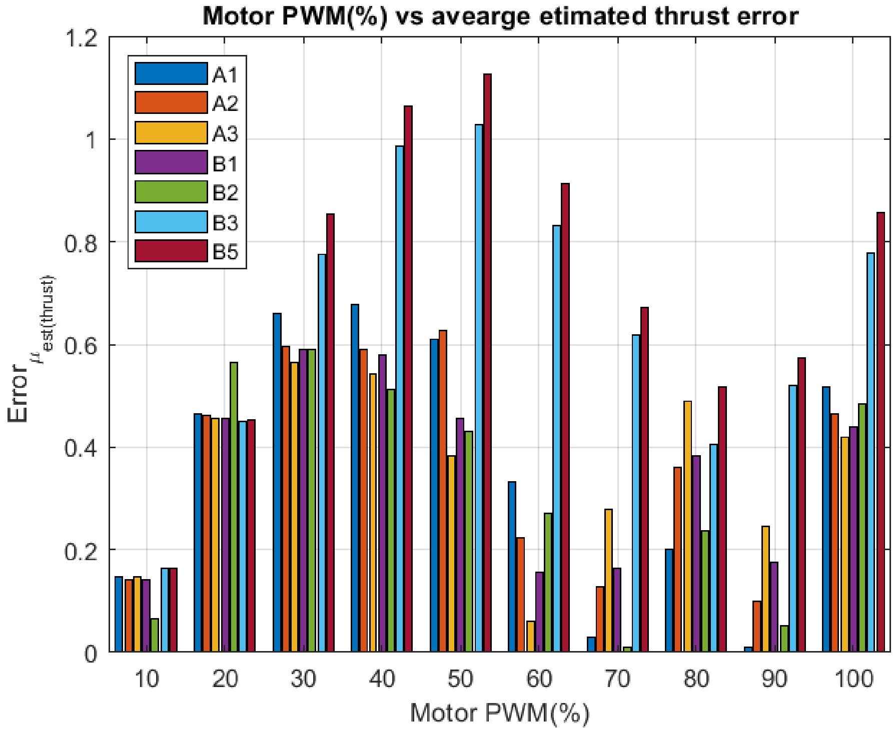

Figure 5.26: Error bar plot showing absolute thrust estimation error when compared with the measured static measurement data obtained in chapter 4.

- The estimated thrust error data does not match with the measurement error data. The error difference is because of the curve fitted error caused by designing a drag torque estimator on noisy drag torque measurement data obtained from the force/torque sensor. It can be concluded that using the suggested estimation method is not a good solution.

5.6 Conclusion

- The analytical design at the static situation has a mean error of 9.02%; this is because of the down-sampling of k_t value, to design a drag estimator.

- The second-order polynomial estimator design at the static situation has a mean error of 7.51%, this is because of curve fitting error caused because of modeling a noisy drag torque measurement data. The measurement noise needs to be removed for better estimation design. Then a non-linear estimator design can be used for better estimation.

- At high PWM signal, i.e., between 60% to 100% the measured thrust and drag torque has high noise because of external wind created by blocking object and the rotating object had a high influence on Force/torque sensor at a motor speed between 60 to 100%. The estimator is designed using current and estimated rotor angular acceleration which has low noise because of the mechanical noise has no influence on ESC which measures current and rotor angular velocity. Hence, estimation has variation between static and other test conditions at higher motor speeds. This influence of mechanical noise can be compensated by designing a closed-loop thrust controller.

- The negative trend in B3 and B5 situations is because the drag torque and thrust were decreasing with an increase in PWM at these situations. This is observed in chapter 4.

- A3 situation as a high error, because of this situation as a high influence of wind, while near the ground. This situation is explained in chapter 4.
- The thrust estimator is designed by using the Matlab curve fitting estimation method.
- The estimated thrust error data has no match with the measurement error data obtained in Table 4.2; this is because of the curve fitting error. It can be concluded that the estimation suggested does not model the noises, besides amplifies it. Eliminating the measurement noise before estimation should produce better results.

6 Conclusion and future work

In this chapter, the conclusions from work done will be presented. Furthermore, some recommendations for future work is also presented.

6.1 Conclusion

The research had three goals sets and the summary of the goals is discussed in this section.

1. Selection of a sensor

   - ESCs use different protocols for communication with FC. The digital protocol as advantages over the other protocols due to its accuracy, high resolution, detection of error signals, and rejecting them. Though this protocol has many advantages, a PWM protocol is used for communication in this thesis because the existing hexacopter used at RAM uses the PWM protocol for communication. Airbot wraith32 ESC is selected because of its embedded sensing capacity, PWM based communication protocol, small size, digital current sensing capability, and high resolution

2. Analyzing the influence of disturbance on a BLDC rotor system

   - The tests were conducted to analyze the influence of disturbances on the rotor system. The tests were divided into two sections, namely, blocking object and rotating object. Nine different disturbance situations were created, and the current, rotor angular velocity, drag torque, and thrust was measured at each of these situations. It was observed that the ground effect had a higher disturbance effect when compared with the other situations, and a mean increase of 9.51% was observed due to the ground effect. This is because the air-flow beneath the propeller gets trapped, increasing pressure beneath the propeller, creating more thrust. When the rotor was placed near the wall, it was seen that it had very less influence of disturbance; a mean thrust of 3.69% was observed at this situation. The ground effect and wall effect had a positive increase in thrust, whereas two rotors placed vertically facing upwards and vertical rotors facing each other had a decrease in thrust measurement. The thrust and drag torque measurements showed high measurement noise in the presence of disturbance; this is because the mechanical sensor also measures the wind disturbances, and motor vibrations. The current, thrust and drag torque has the same trend, but rotor angular velocity has an opposite trend; this is because of the increase in torque results in decreasing angular velocity. The analysis chapter helped to understand the effect of wind on the propeller system. Though the factor of disturbance was less, designing a closed-loop thrust control will help in accurate thrust control, in tasks that require precision.

3. Thrust estimator design

   - A drag torque estimator was designed, using an analytical and curve-fitting model. The analytical model was based on the system's physical model, along with using the rotors acceleration and motor current acquired from embedded sensors. The design had a 9.02% error when compared with the static condition model. The error was because of the down-sampling of the k_t parameter. To-overcome this error a second-order polynomial estimator was designed using the MATLAB curve fitting method; this method showed a mean error of 7.51% due to the curve fitting error because of modeling a noisy signal. The estimator design also showed high variations for motor speed between 60 to 100%; this is because of wind disturbance influence on drag torque measurements showed high measurement noises. This noise influence can be reduced by designing a closed-loop thrust controller. The thrust estimator was designed using proportional relation between thrust and estimated drag torque. The estimator followed the same trend has the drag torque estimator because the thrust measurement as a direct influence of drag torque, i.e., The thrust estimator is a static map of estimated drag torque. It was observed that the estimated thrust data had no match with the measurement data. Hence, a better thrust estimation model needs to be designed for better estimation.

6.2 Future work

After this work, there are some points on which the work is required,

- The PWM signal used at present can be replaced by Dshot1200 protocol for fast communication between flight controller and ESC, the Dshot protocol will also decrease the communication delay created by the control-loop, increases accuracy, rejects error signals, high resolution and smaller size.
- It was observed that the Force/torque sensor had high noise, to design a better estimator the noise must be removed from the measured data. The noise in the measurement tis due to motor vibrations, the thrust generated by the propeller will try to lift the setup creating more oscillations in measurement data. The second type of noise is because of the wind flowing through the rotor. All these measurement noise needs to be separated before designing the estimator.
- A better estimator can be designed by using a non-linear estimator design.
- It was observed that the rotor angular acceleration had very less influence on drag torque estimation because of lower motor moment of inertia, for better results a drag torque estimator can be designed using current as input.
- After a better design of estimator a closed-loop thrust controller is needed for accurate measurement of thrust.
- Another solution for the problem would be using Kalman filter based on sensor fusion for estimating thrust and POSE of interactive UAV [51]. The sensors that can be used to measure the POSE are LIDAR or IMUs.

Bibliography

[1] V. Kumar R. Mohony and P. Corke. Multirotor aerial vehicles: Modeling, estimation, and control of quadrotor. In Robotics Automation Magazine, editor, *ARPN Journal of Engineering and Applied Sciences 2016*, volume 19 of *Concurrent Systems Engineering Series*, pages 20–32. IEEE Robotics Automation Magazine, September 2012.

[2] Q. Wang. The current research status and prospect of multi-rotor uav volume = 14, year = 2017, pages = "31-35", publisher = "iosr journal of mechanical and civil engineering (iosr-jmce)",. August.

[3] T. Howard T. Nguyen M. Frietsch A. Albers, S. Trautmann and C. Sauter. Semi-autonomous flying robot for physical interaction with environment.

[4] N. Stilinovic Q. Zhang D. Reusser I. Sa J. Nieto R. Siegwart A.S. Vempati, M.S. Kamel and P. Beardsley. Paintcopter: An autonomous uav for spray painting on 3d surfaces. 2017.

[5] J.P.(Just) van Westerveld. *Investigating the Usability of a Novel Type of Sensing for Aerial Vehicles*. University of Twente, Internship report, 2016.

[6] Rami A. Mattar and R. Kalai. Development of a wall-sticking drone for non-destructive ultrasonic and corrosion testing. volume 8. MDPI journals, 2012.

[7] ZACC DUKOWITZ. Flyability Releases Elios 2 at AUVSI XPONENTIAL, Positioned to Be Best Indoor Inspection Solution on the Market. https://uavcoach.com/elios-2/.

[8] H.H.Bulthoff M.Ryll and P.R.Giordano. A novel overactuated quadrotor uav: Modeling, control and experimental validation.

[9] C. Scott Marchman. Thrust sensing for small uavs. Master thesis.

[10] E. Davis and P. E. Pounds. Direct thrust and velocity measurement for a micro uav rotor.

[11] E. Davis and P. El Pounds. Direct sensing of thrust and velocity for a quadcopter rotor array. volume 2, pages 1360–1366. IEEE Robotics Automation Magazine, July 2017.

[12] P. Martin and E. Salun. The true role of accelerometer feedback in quadrotor control. pages 1623–1629. IEEE International Conference on Robotics and Automation, September 2010.

[13] Myunggon Yoon. A automatic thrust measurement system for multi-rotor helicopters. volume 4. International journal of engineering technology(IJERT), December 2015.

[14] B. Arain and F. Kendoul. Real-time wind speed estimation and compensation for improved flight. volume 50, pages 1509–1606. IEEE Transactions on Aerospace and Electronic Systems, April 2014.

[15] Nitin D. W. Yeo and D. A. Paley. Onboard flow sensing for downwash detection and avoidance with a small quadrotor helicopter. American institute of aeronautics and astronautics, 2010.

[16] NASA. *Principles of flight*. National Aeronautics and Space Administration, 2010.

[17] NASA. What is Lift. https://www.grc.nasa.gov/WWW/K-12/airplane/lift1.html.

[18] Wikipedia. Lift (force). https://en.wikipedia.org/wiki/Lift_(force).

[19] J. G Leishman. *Principles of helicopter aerodynamics*. Cambridge Aerospace Series, 2000.

[20] U.S department of transportation. *Rotor flying handbook*. Fedral aviation Administration, 2000.

[21] Wikipedia. Camber (aerodynamics). https://en.wikipedia.org/wiki/Camber_(aerodynamics).

[22] Wikipedia. Airfoil. https://en.wikipedia.org/wiki/Airfoil.

[23] Wikipedia. Bernoulli's principle. https://en.wikipedia.org/wiki/Bernoulli%27s_principle.

[24] Federal aviation administration. *Helicopter ying handbook,.* U.S. Department of Transportation Federal aviation administration flight standards service, 2012.

[25] NASA. What is thrust? https://www.grc.nasa.gov/WWW/k-12/airplane/thrust1.html.

[26] Prouty. *Helicopter performance, stability, and control.* Krienger Publishing Company, 1995.

[27] Nathalie Nowicki. Measurement and modeling of multicopter UAS rotor blade deflection in hover. KTH - Royal Institute of Technology, July 2016.

[28] Parolini Zagaglia Gibertini, Grassi and Zanotti. Experimental investigation on the aerodynamic interaction between a helicopter and ground obstacles. In Proceedings of the Institution of Mechanical Engineers, editor, *Journal of Aerospace Engineering*, volume 229, pages 1395–1406, September 2015.

[29] C.T Lao and E.T.T. Wong. Cfd simulation of a wing-in-ground-effect uav. In *International Conference on Aerospace and Mechanical Engineering,*, volume 370. IOP publications, 2017.

[30] Yun L and Bliault. *Ground Effect Craft Technology.* New York: Springer, 2010.

[31] V. Kumar and N. Michael. Opportunities and challenges with autonomous micro aerial vehicles. volume 31, pages 1279–1291. The International Journal of Robotics Research, September 2012.

[32] I.C Cheeseman and W.E Bennett. The effect of the ground on a helicopter rotor in forward flight. Aeronautical Research Council, September 1995.

[33] Harry H. Heyson. The effect of wind-tunnel wall interference on the performance of a fan-in-wing vtol model. NASA Langley research center, February 1974.

[34] Johan Engelen Ramy Rashad, Petra Kuipers and Stefano Stramigioli. Design, modeling, and geometric control on se(3) of a fully-actuated hexarotor for aerial interaction. arXiv.org, September 2017.

[35] Ramond Prouty. Helicopter performance, stability, and control. Krieger Publishing Company, 1995.

[36] E. B. Davis. Aerodynamic force interactions and measurements for micro quadrotors. The University of Queensland, Australia, nov 2018.

[37] E. Kuantama and R. Tarca. Quadcopter thrust optimization with ducted-propeller. volume 126. Annual Session of Scientific Papers, IMT ORADEA, 2017.

[38] J. S. B. G. M.V.Ramesh. "speed torque characteristics of brushless dc motor in either direction on load using arm controller. In *Journal of Energy Technologies and Policy*, volume 2, September 2011.

[39] D. C. Hanselman. *Brushless Permanent Magnet Motor Design.* Magna Physics Publishing, 2006.

[40] What are Brushless DC Motors. https://www.renesas.com/us/en/support/technical-resources/engineer-school/brushless-dc-motor-01-overview.html.

[41] J. W. Dixon and I. A. Leal. "current control strategy for brushless dc motors". In *IEEE TRANSACTIONS ON POWER ELECTRONICS,*, volume 17, pages 232–240, March 2002.

[42] Elprocus. Introduction To Electronic Speed Control (ESC) Working and Applications. https://www.elprocus.com/electronic-speed-control-esc-working-applications/.

[43] H. Edward O. Natalie E. George, S. Chetan. A study of the degradation of electronic speed controllers for brushless dc motors. Asia Pacific conference of the prognostics and health management society, 2017.

[44] Oscar Liang. BLHELI32 ESC FIRMWARE OVERVIEW. https://oscarliang.com/blheli-32-overview/.

[45] Cobra C-2217/20 Brushless Motor, Kv=960. https://innov8tivedesigns.com/cobra-c-2217-20-brushless-motor-kv-960.

[46] T-Motor. 11 ∗ .37. https://hobbyking.com/en_us/multirotor-carbon-fiber-t-style-propeller-11x3-7-black-cw-ccw-2pcs.html?___store=en_us.

[47] Arduino UNO. https://store.arduino.cc/arduino-uno-rev3.

[48] ATI. F/T Sensor: Mini40. https://www.ati-ia.com/products/ft/ft_models.aspx?id=Mini40.

[49] M. Kenderova I. Virgala, P. Frankovsky. Friction Effect Analysis of a DC Motor. pages 1–5. American Journal of Mechanical Engineering, 2013.

[50] Y. Ma C. Xiang, X. Wang and B. Xu. "practical modeling and comprehensive system identification of a bldc motor". In *Hindawi Publishing Corporation Mathematical Problems in Engineering*, March 2015.

[51] N. Michael S. Shen and V. Kumar. "obtaining liftoff indoors: Autonomous navigation in confined indoor environments". In *IEEE Robot. Automation Magazine*, volume 20, pages 40–48, December 2013.